In Situ Infrared Attenuated Total Reflection (IR ATR) Spectroscopy: A Complementary Analytical Tool for Drug Design and Drug Delivery

Urs Peter Fringeli*

Urs Peter Fringeli. Born November 26, 1939 in Basel, Switzerland. 1959–63 Study of Natural Sciences at the ETH-Zürich. Diploma work in Physical Chemistry. 1964–69: Doctorate at the Laboratory for Physical Chemistry of ETH with Prof. *Hs. H. Günthard.* Thesis: 'Construction of an Infrared-Modulation-Spectrometer for the Measurement of Absorption and Life-time of Photochemically Excited States.' 1970–72: Postdoctoral fellow at the *Max-Planck*-Institute for Biophysical Chemistry, Göttingen (Prof. *M. Eigen*), and at the *Battelle* Institute, Geneva (Prof. *W. Leuzinger*). 1972–83: Project leader in Prof. *Günthard*'s group at the Laboratory for Physical Chemistry, ETH-Zürich. Field: Molecular Structure of Biomembranes. Method: Infrared-ATR Spectroscopy. Lectures in Biophysical Chemistry. 1977: Privatdozent, 1979: *Ruzicka* award of the Council of Swiss Federal Institutes of Technology. Since 1984: Professor for Applied Physical Chemistry and Biophysical Chemistry at the University of Vienna. Academic guest at the Laboratory for Physical Chemistry of ETH-Zürich.

Abstract. A comprehensive summary of basic relations for quantitative IR ATR spectroscopy of isotropic and oriented samples is given. Experimental requirements for detection of sub-monolayer quantities in aqueous environment are discussed. New instrumental developments such as a single-beam-sample-reference (SBSR) attachment, and FTIR modulation spectroscopy at low frequencies are presented. Examples of *in situ* experiments with tertiary-amine local anesthetics interacting with planar, immobilized lipid bilayers are discussed. Partition coefficients of the total amine, as well as of the protonated and deprotonated forms have been determined. Structural alterations, especially of lipids, were detected upon interaction. Adsorption isotherms revealed multilayer formation at the membrane surface. The onset of this process for dibucaine is at *ca.* 5 mM bulk concentration or even below. Preferential accumulation of dibucaine base is observed already at bulk pH 5.5 (pK_a = 8.83). For peptide conformation analysis, FTIR temperature (T) modulation experiments were performed for the first time. A modulation amplitude of $\Delta T = \pm 1°$ at a given mean temperature is shown to result in high-quality phase-resolved spectra enabling detailed insight into periodically induced changes of the state of the sample.

Introduction

In the past decade, *Fourier*-transform IR (FTIR) spectrometers have replaced dispersive instruments because of their better performance in nearly all respects [1]. The problem of background compensation e.g. could be reduced significantly, enabling routine measurements even in aqueous environment. Therefore, a growing interest in IR membrane spectroscopy was observed from the biophysical, biochemical, and biomedical viewpoints [2–39] as well as from the biosensor part [40][41]. The works cited here have to be considered as typical examples just available to the author at present. Since the aim of this article is presenting ATR techniques for *in situ* experiments as well as the theoretical background for quantitative analysis and orientation measurement, rather than reviewing papers published so far, the reader is also referred to the reference lists of cited papers. In most of these papers conventional transmission (T) technique has been used, perhaps because for simple applications sample preparation and data interpretation may be easier than with ATR technique. The latter, however, has significant advantages over T spectroscopy, especially with respect to structure determination under *in situ* conditions.

Sect. 2 gives a comprehensive introduction into the principles of ATR spectroscopy, wheras *Sect. 3* deals with experimental considerations, such as sensitivity requirements, background compensation and modulation spectroscopy. *Sect. 4* gives a summary of typical applications like preparation of model membranes and living cells for *in situ* experiments, interaction of local anesthetics with lipid bilayers, determination of partition coefficients between membrane and aqueous environ- ment, as well as temperature modulation. The latter enables access to conformational equilibria of polypeptids and lipids. Besides of utmost background compensation, modulation spectroscopy enables kinetic analysis, too, provided that the circular modulation frequency ω_m and the rate constants of excited reactions are of the same magnitude. The situation is optimum, when the response of the sample is fully reversible [42–46]. Estimates reveal that signal to noise (S/N) enhancement by this technique should be sufficient to get information on the molecular structure of a substrate molecule bound to its specific receptor under *in situ* conditions. Such data are of predominant interest in drug design.

2. Principles of ATR Spectroscopy

2.1. Basic Phenomena

Fig. 1 shows a schematic comparison of the conventional transmission (*a*) and the internal reflection (*b*) technique. The latter is achieved by placing the sample

Correspondence: Prof. U.P. Fringeli
University of Vienna
Währingerstrasse 42
A–1090 Vienna
and Institute for Physical Chemistry
ETH-Zentrum
CH–8092 Zürich

material in close contact with the optically transparent internal reflection element (IRE) of higher refractive index and working above the critical angle θ_c.

Under these conditions, it follows that an electromagnetic field still exists in the rare medium beyond the reflecting interface. This field exhibits the frequency of the incoming light, but the amplitude falls off exponentially with distance z from the surface.

$$E = E_o e^{-z/d_p} \tag{1}$$

d_p denotes the depth of penetration and is given by

$$d_p = \frac{\lambda_1}{2\pi (\sin^2\theta - n_{21}^2)^{1/2}} \tag{2}$$

n_{21} stands for the ratio n_2/n_1 of the refractive indices of the rarer medium (n_2) and of the internal reflection element (n_1). λ_1 denotes the wavelength λ_{vakuum}/n_1 in the latter. According to Eqn. 2, the penetration depth amounts to the order of magnitude of the wavelength λ_1 of the IR radiation in the IRE. Fig. 2 schematically represents the situation when a thin film (e.g. a bilayer or a protein layer) is immobilized at the surface of the IRE. This is a typical set-up for in situ membrane and biosensor studies. The displacement D, the so-called Goos-Hänchen displacement [48] is also in the order of λ_1.

The 'evanescent wave' exhibits another interesting feature, namely the existence of electric field components along all three axis of the rectangular coordinate system attached to the ATR plate (Fig. 3). In contrast, the incident plane wave has only electric field components perpendicular to the direction of propagation. By means of a polarizer, two distinct directions of the incident electric-field vector may be chosen, namely parallel ($\parallel$, pp) and perpendicular ($\perp$, vp) to the plane of incidence (x,z plane). For geometrical reasons (see Fig. 3) it follows that $E_\parallel$ results in the E_x and E_z, and $E_\perp$ the E_y component of the evanescent field.

The relative electric field components in the rarer medium 2 at $z = 0$ (1,2 interface), i.e. the ratio between the electric-field components E_{02x}, E_{02z}, E_{02y} and $E_{01\parallel}$, $E_{01\perp}$ are given by Fresnel's equations [49]. Eqns. 3–5 hold exactly for non-absorbing media 1 and 2, but they are good approximations for weak absorbing samples [46][47]. This condition is fulfilled for all types of experiments reported in this article [46].

The relative electric field components in a thin film of thickness $d \ll d_p$ (see Fig. 2) are given by:

$$E_{02x}^r = E_{02x}/E_{01\parallel} = \frac{2\cos\theta(\sin^2\theta - n_{31}^2)^{1/2}}{(1 - n_{31}^2)^{1/2}[(1 + n_{31}^2)\sin^2\theta - n_{31}^2]^{1/2}} \tag{3}$$

$$E_{02z}^r = E_{02z}/E_{01\parallel} = \frac{2\cos\theta n_{32}^2 \sin\theta}{(1 - n_{31}^2)^{1/2}[(1 + n_{31}^2)\sin^2\theta - n_{31}^2]^{1/2}} \tag{4}$$

$$E_{02y}^r = E_{02y}/E_{01\perp} = \frac{2\cos\theta}{(1 - n_{31}^2)^{1/2}} \tag{5}$$

with $E_{02\parallel}^r = (E_{02x}^{r2} + E_{02z}^{r2})^{1/2}$, and $E_{02\perp}^r = E_{02y}^r$.

n_{ik} denotes the ratio of refractive indices n_i/n_k of medium i and k, where $i, k = 1, 2,$ and 3 stand for ATR plate, thin films and surrounding medium, respectively. For bulk rarer medium $d \gg d_p$ (see Fig. 2) index 3 must be replaced by 2. It should be noted, that generally E_{0x}^r, E_{0y}^r, and E_{0z}^r are not equal.

The relative electric-field strength for intermediate layer thickness ($d \approx d_p$) may be approximated by the Interpolation 6.

$$E_{02}^r(d) = E_{02}^r(th) + (1 - e^{-d/d_p}) \cdot (E_{02}^r(bu) - E_{02}^r(th)) \tag{6}$$

where th and bu denote 'thin layer', and 'bulk', respectively. For $d \to 0$ Eqn. 6 results in Eqns. 3–5 for thin layers, and for $d \to \infty$ one obtains the electric-field components in a bulk rarer medium (Eqns. 3–5 with $n_3 = n_2$).

2.2. Quantitative Analysis of Isotropic Samples

Quantitative analysis in transmission spectroscopy is based on Lambert-Beer's law

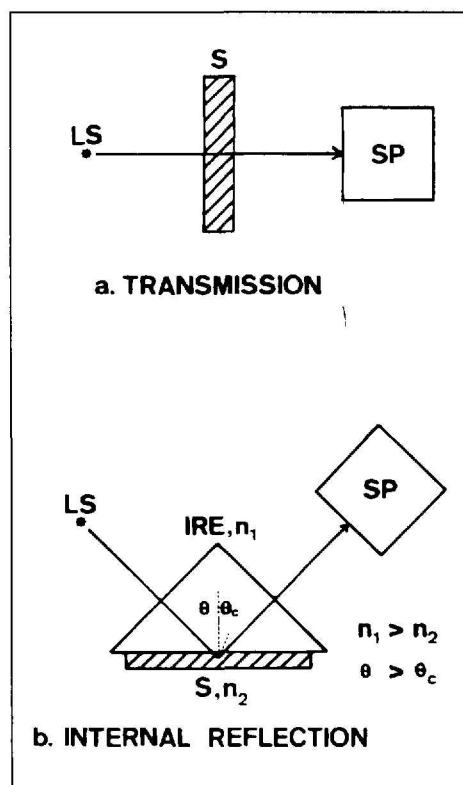$$T = I_S/I_o = 10^{-A} = 10^{-\varepsilon cd} \tag{7}$$

Fig. 1. Comparison of transmission (a) with internal reflection (b) technique. LS: light source, S: sample, SP: spectrometer, IRE: internal reflection element (ATR crystal), θ: angle of incidence, θ_c: critical angle, n_1, n_2: refractive index of IRE and S, respectively.
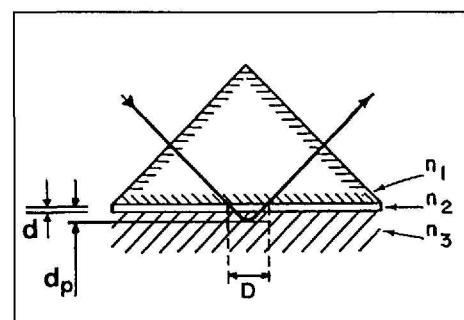

Fig. 2. Measurements on thin films. The penetration depth d_p is larger than the film thickness d. n_1, n_2, n_3 denote the refractive indices of IRE, film and bulk environment, respectively. The penetrating ray is displaced by the distance D [48].
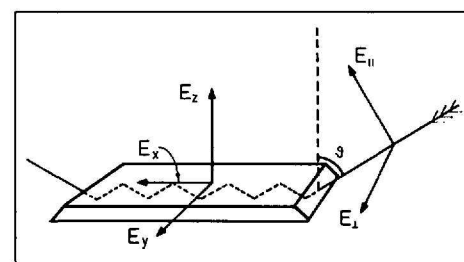

Fig. 3. ATR set-up for multiple internal reflections (MIR). θ, angle of incidence; $E_\parallel$, $E_\perp$, parallel and perpendicular polarized components of the electric field of incident light. E_x, E_y, E_z, electric-field components with respect to the plate-fixed coordinate system. ($E_\parallel \to E_x, E_z, E_\perp \to E_y$, see [46][47]). From [2].

The meaning of the symbols are transmittance (T), intensity before (I_o) and after (I_S) the sample, absorbance (A), molar absorption coefficient (ε), molar concentration (c), and sample thickness (d), respectively. To apply *Lambert-Beers*'s law to ATR data, one has to introduce a hypothetical thickness d_e of a sample which would result in the same absorbance of a given band *via* transmission as obtained with the real sample thickness d in the ATR experiment. The quantity d_e was introduced by *Harrick* [47] and referred to as 'effective thickness'.

For the limiting cases 'bulk medium 2' ($d = \infty$), and 'thin layer' ($d \ll d_p$) one obtains

$$d_e = \frac{1}{\cos\theta}\frac{n_2}{n_1}\frac{d_p}{2}E_{02}^{r2} \text{ and} \quad (8)$$

$$d_e = \frac{1}{\cos\theta}\frac{n_2}{n_1}d\,E_{02}^{r2}, \text{ respectively} \quad (9)$$

It should be noted that d_e for a bulk medium increases linearly with wavelength λ (see *Eqn. 2*), whereas d_e for a thin film does not depend on λ. The effective thickness for an intermediate sample thickness ($d \approx d_p$) may be calculated by using *Eqn. 6*. For more details, on effective thickness, see [46]. As a consequence of the application of *Fresnel*'s equations, simple application of *Lambert-Beer*'s law to ATR data requires polarized incident light [46],

$$T_{\|} = 10^{-\varepsilon c d_{e\|}} = 10^{-A_{\|}}, \text{ and}$$
$$T_{\perp} = 10^{-\varepsilon c d_{e\perp}} = 10^{-A_{\perp}} \quad (10)$$
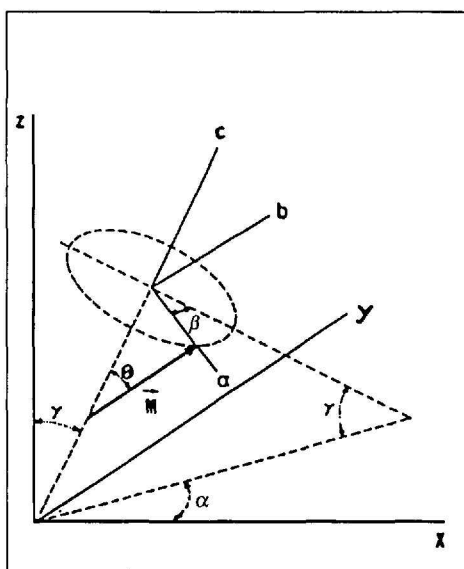

Fig. 4. *Partial axial orientation.* Molecular axis c forms angle γ with z axis of the ATR plate-fixed coordinate system x,y,z. a,b,c is the molecule-fixed coordinate system. α, β, and γ are the *Eulerian* angles. From [51].

2.3. Quantitative Analysis of Oriented Samples

In the case of an oriented sample, the absorbance depends not only on the number of particles per volume (or area) but also on the structure of the sample. For that reason, quantitative analysis of an oriented sample means both, determination of concentration and orientation.

2.3.1. Orientation Measurements

For a comprehensive discussion of orientation measurements in transmission spectroscopy, see [50–52].

2.3.2. Theory of Integrated Absorbance of Oriented Samples

The integrated absorbance is proportional to the square of the scalar product between the transition dipole moment $\vec{M}$ and the electric field $\vec{E}$ of radiation. For the case of excitation of one quantum of the k-th normal mode q_k from the ground state, $\vec{M}$ is proportional to the change $(\delta\vec{\mu}/\delta q_k)_o$ of the molecular dipole moment $\vec{\mu}$ with respect to the normal mode displacement q_k [53].

$$A(\bar{\upsilon})d\bar{\upsilon} = cd \cdot \int \varepsilon(\bar{\upsilon})d\bar{\upsilon}\,\alpha\,(\vec{M}\cdot\vec{E})^2, \quad (11)$$

band

where

$$(\vec{M}\cdot\vec{E})^2 = |\vec{M}|^2|\vec{E}|^2\cos^2(\vec{M},\vec{E}) =$$
$$(M_xE_x+M_yE_y+M_zE_z)^2 \quad (12)$$

Eqns. 11 and *12* form the basis of orientation measurements.

2.3.3. Ultrastructure

Two problems have to be solved in order to get structural information. First, the relative orientation of the ATR plate fixed coordinate system (x,y,z) and the molecular coordinate system (a,b,c) must be known. This is equivalent to the knowledge of the ultrastructure of the molecular entity. Secondly, the knowledge of the orientation of the transition dipole moment $\vec{M}$ (M_a,M_b,M_c) within the molecule is a prerequisite for molecular-structure analysis. This requirement often limits the application of the analytical procedure described below to typical vibrations of functional groups, unless more details on the direction of $\vec{M}$ are available via normal coordinates analysis [53].

The angles α, β and γ are the *Eulerian* angles, enabling description of the mutual position of the two coordinate systems. Transformation of (M_a,M_b,M_c) into (M_x,M_y,M_z) is performed by the matrix *Eqn. 13*.

$$\begin{pmatrix} M_x \\ M_y \\ M_z \end{pmatrix} = \begin{pmatrix} \cos\beta\cos\gamma\cos\alpha + \sin\beta\sin\alpha \\ \cos\beta\cos\gamma\sin\alpha - \sin\beta\cos\alpha \\ -\sin\gamma\cos\beta \end{pmatrix}$$

Thus, if (M_a,M_b,M_c) are known from experience or from normal coordinates analysis [53] (M_x,M_y,M_z) are calculated by coordinate transformation (*13*) and inserted into *Eqns. 11* and *12*. The electric-field components are given by *Eqns. 3–6*. Obviously, this procedure results in a quantity which is proportional to the integrated absorbance, however, for most samples this is only a fractional contribution, since the entity of molecules exhibit a certain distribution with respect to the *Eulerian* angles, which is typical for a given ultrastructure. For definition of ultrastructures see [45][46]. Typical features of biomembranes are random arrangement of molecules around a space-fixed axis normal to the plane of the membrane (z axis) and free rotation around the molecular axis (c axis) as well as fluctuation of the angle γ between molecular axis and space-fixed axis (*Fig. 4*). This ultrastructure is referred to as liquid crystalline ultrastructure (LCU) and is characterized by isotropy with respect to α and β. whereas γ exhibits a distribution around a mean value γ_o ($0° \le \gamma \le 90°$).

The fluctuation of the molecular axis (c) with respect to the space fixed axis (z) is described by the distribution function $f(\gamma)$ [51][52][54].

2.3.4. Dichroic Ratio and Order Parameter

The relevant parameter in most optical orientation measurements is the dichroic ratio R

$$R = \frac{A_{\|}}{A_{\perp}} = \frac{\int A_{\|}(\bar{\upsilon})\,d\bar{\upsilon}}{\int A_{\perp}(\bar{\upsilon})d\bar{\upsilon}} \quad (14)$$

$A_{\|}$ and $A_{\perp}$ denote the peak absorbances of a given band for parallel (‖) and perpendicular ($\perp$) polarized incident light, respectively. Following the path described above, the axial absorbances A_x, A_y, and A_z can be calculated for a given ultrastructure. The procedure has been described in details for transmission spectroscopy by *Zbinden* [51] and *Michl* and *Thulstrup* [52]. Adaptation to ATR spectroscopy is straightforward and has been done selecting the y axis [55] and the z axis [45][46] as space-fixed axis of a LCU. In the latter case, the axial absorbances are given by

$$\begin{pmatrix} \sin\beta\cos\gamma\cos\beta - \cos\beta\sin\alpha & \cos\alpha\sin\gamma \\ \sin\beta\cos\gamma\sin\alpha + \cos\beta\cos\alpha & \sin\alpha\sin\gamma \\ -\sin\gamma\sin\beta & \cos\gamma \end{pmatrix} \begin{pmatrix} M_a \\ M_b \\ M_c \end{pmatrix} \tag{13}$$

$$A_x = \frac{1}{3}\alpha\mid\vec{M}\mid^2 E_{02x}^{r2}\,[1 - \frac{1}{2}S(3\cos^2\Theta - 1)] = \varepsilon c d_{ex} N \tag{15}$$

$$A_y = \frac{1}{3}\alpha\mid\vec{M}\mid^2 E_{02y}^{r2}\,[1 - \frac{1}{2}S(3\cos^2\Theta - 1)] = \varepsilon c d_{ey} N \tag{16}$$

$$A_z = \frac{1}{3}\alpha\mid\vec{M}\mid^2 E_{02z}^{r2}\,[1 + S(3\cos^2\Theta - 1)] = \varepsilon c d_{ez} N \tag{17}$$

Θ and N denote the angle between the tansition moment $\vec{M}$ and the molecular axis c, and the number of active internal reflections, respectively. The parameter S, the so called order parameter, is defined according to (18)

$$S = \frac{3}{2}\int_0^{\pi/2} f(\gamma)\cos^2\gamma\,\mathrm{d}\gamma - \frac{1}{2} \tag{18}$$

$f(\gamma)$ is the distribution function (probability density) for the molecular axis c (see *Fig. 4*) with respect to a space fixed axis (*e.g.* z axis). Since an isotropic sample exhibits $f(\gamma) = \sin\gamma$, it follows from *Eqn. 18* that the corresponding order parameter becomes zero ($S_{iso} = 0$). On the other hand, a perfect alignment of the molecular axis along the z axis results in $f(\gamma) = \delta(\gamma)$, leading to a corresponding order parameter of $S = 1$. Fluctuation of the c axis with respect to the z axis will reduce the order parameter correspondingly. Thus, for a LCU it follows $0 < S < 1$. It should be noted that, in a more general picture [56–58], S corresponds to the diagonal element S_{zz} of the order parameter tensor S. For LCU one obtains

$$S = S_{zz} = -2 S_{xx} = -2 S_{yy} \tag{19}$$

which is confirmed by *Eqns. 15–17*. Introducing *Eqns. 15–17* into *Eqn. 14* by taking into account that $A_\| = A_x + A_z$, and $A_\perp = A_y$, one obtains for the dichroic ratio with respect to the z axis

$$R_z^{ATR}(LCU) = \frac{E_{02x}^{r2}}{E_{02y}^{r2}} + \frac{E_{02z}^{r2}}{E_{02y}^{r2}} \frac{1 + S(3\cos^2\Theta - 1)}{1 - \frac{1}{2}S(3\cos^2\Theta - 1)} \tag{20}$$

Finally, it should be mentioned that structural features as revealed by *Eqns. 15--17* and *Eqn. 20* are expressed by the orientation function

$$\sigma = S(3\cos^2\Theta - 1) \tag{21}$$

As a consequence, in a LCU picture as descirbed above determination of both, S and Θ is not possible by a single dichroic ratio of a given band. It requires the analysis of the dichroic ratios of at least two absorption bands (1,2) resulting from the same functional group. Since in this case $S_1 = S_2 = S$, and in a given (assumed) orientation Θ_1 and Θ_2 are related for geometrical reasons, it is possible to determine both, the order parameter (fluctuation) and the mean spacial orientation of the corresponding functional group. Good estimates of the direction of $\vec{M}$ (M_a, M_b, M_c) (see *Fig. 4*) are known for a number of functional groups [45], such as $\upsilon_s(CH_2)$, $\upsilon_{as}(CH_2)$, $\delta(CH_2)$, $\gamma_w(CH_2)$, $\gamma_r(CH_2)$; $\upsilon_{as}(COO^-)$, $\upsilon_s(COO^-)$; $\upsilon(C=O)$, $\upsilon(COO)$; $\upsilon_{as}(PO_2^-)$, $\upsilon_s(PO_2^-)$ *etc.* Combination of *Eqns. 20* and *21* results in

$$R_z^{ATR}(LCU) = \frac{E_{02x}^{r2}}{E_{02y}^{r2}} + \frac{E_{02z}^{r2}}{E_{02y}^{r2}} \frac{1 + \sigma}{1 - \frac{1}{2}\sigma} \tag{22}$$

In a recent paper, *Hübner* and *Mantsch* [38] have derived a formalism for the analysis of polarized ATR spectra of LCU

samples aligned along the z axis. The relevant quantity for orientation measurement was reported to be $f = \frac{1}{2}(3\cos^2\beta - 1)$ and referred to as 'order parameter'. β denotes the mean angle between the z axis and the molecular axis. From the definition of the order parameter (*Eqn. 18*), which is the same as in [38], it follows that the expression $f = \frac{1}{2}(3\cos^2\beta - 1)$ can only result for a distribution function $\delta(\gamma - \beta)$ (see *Eqn. 18*). This means, however, that any molecular fluctuation is excluded, which is equivalent to setting the order parameter $S_{zz} = S = 1$ (*Eqn. 19*). Analysis of polarized ATR spectra of LCU systems by the formalism given in [38] may, therefore, lead to significant systematic errors. Let *e.g.* R_1 and R_2 be the dichroic ratios of equal functional groups at different positions in a molecule. $R_1 = R_2$ only means same orientation for both groups, if $S_1 = S_2$. If, however, $S_1 \neq S_2$, which means different fluctuation behaviour, one has to conclude different spacial orientations. On the other hand, if $R_1 \neq R_2$ and $S_1 \neq S_2$ both groups may still have the same mean orientation. Consequently, the orientational accuracy claimed in [38] is not substanciated.

2.3.5. *Dichroic Ratio of Overlapped Bands*
i) *Different Degrees of Ordering*

A situation often found in polypeptide- and hydrocarbon-chain spectroscopy is a superposition of typical absorption bands (*e.g.* amide I,II, CH_2 stretching, bending, rocking). This leads to an overall dichroic ratio which is experimentally accessible. It depends on the orientation of each associated functional group. Separation by any line-shape analysis procedure is mostly not possible. A good estimation of the amount and orientation of one component can be obtained, however, when mole fraction and orientation of the other components are known [59–61]. *Eqn. 23* is at least a good tool to calculate the dichroic ratio of a composed band *i.e.* to assess an expected molecular conformation with respect to its consistency with experimental data.

$$R_z^{ATR} = \frac{A_\parallel}{A_\perp} = \frac{\sum_{i=1}^{n} x_i m_i^2 \{E_{02x}^2[1-\frac{1}{2}\sigma_i] + E_{02z}^2 [1 + \sigma_i]\}}{\sum_{i=1}^{n} x_i m_i^2 E_{02y}^2[1-\frac{1}{2}\sigma_i]} \qquad (23)$$

x_i and m_i denote the mole fraction and the relative transition moment $(m_i=|\vec{M}_i|/|\vec{M}_1|)$. σ_i is the orientation function of the i-th segment as defined by *Eqn. 21*.

ii) *Dichroic Difference Spectra*

This is a method which enables subtraction of the random component from the whole band. The procedure is of general practical interest, because it helps localizing orientated regions in a molecule. Dichroic difference spectra $A^* (\tilde{v})$ are weighted difference spectra between parallel polarized $A_\parallel(\tilde{v})$ and perpendicular polarized $A_\perp(\tilde{v})$ absorbance spectra of the same sample, *i.e.*

$$A^* (\tilde{v}) = A_\parallel (\tilde{v}) - R_{iso}A_\perp(\tilde{v}) \qquad (24)$$

where R_{iso} denotes the dichroic ratio of an isotropic sample. Obviously, in the dichroic difference spectrum $A^*(\tilde{v})$, all absorption bands resulting from isotropically oriented transition dipole moments are eliminated. *Eqn. 24* has been used for the subtraction of the random part of protein spectra [2][28][60]. Details on the practical procedure are given in [46].

2.4. *Determination of Surface Concentration*

The concept of 'effective thickness' (see above) is maintained also for oriented samples. However, one has to take into account that the effective thickness may become zero (no absorbance), if the angle between the transition dipole moment $\vec{M}$ and the electric-field vector $\vec{E}$ is 90°, and maximum for parallel alignment of the two vectors. Weighting is achieved by multiplying the axial effective thicknesses obtained for an isotropic sample by factors depending on the ultrastructure of the sample.

In the case of LCU with predominant alignment along the z axis, the axial absorbances $A_x, A_y,$ and A_z are given by *Eqns. 15–17* with $A_\parallel = A_x + A_z$ and $A_\perp = A_y \cdot A_\parallel$ and $A_\perp$ are experimentally available. Obviously, the expressions within brackets are the typical features of LCU/z. The weighting factors for axial effective thicknesses of an oriented sample are, therefore, given by

$$W_{xy} = 1 - \frac{1}{2} S (3\cos^2\Theta-1) = 1 - \frac{1}{2} \sigma \quad(25)$$

and

$$W_z = 1 + S (3\cos^2\Theta - 1) = 1 + \sigma \quad (26)$$

Eqns. 25 and 26 become unity in the isotropic case $S = 0$. Therefore,

$$d_{ex} = W_{xy}d_{ex}^{iso}, \, d_{ey} = W_{xy}d_{ey}^{iso}$$
$$d_{ez} = W_z d_{ez}^{iso} \qquad (27)$$

with

$$d_{e\parallel} = d_{ex} + d_{ez}, \text{ and } d_{e\perp} = d_{ey} \qquad (28)$$

where $d_{ex}^{iso}, d_{ey}^{iso},$ and d_{ez}^{iso} denote axial effective thicknesses of an isotropic sample (*Eqns.* 8 and 9). For the concentration of an oriented sample one obtains

$$c = \frac{A_\parallel}{vN\varepsilon d_{e\parallel}} = \frac{A_\perp}{vN\varepsilon d_{e\perp}}, \text{ or} \qquad (29a)$$

$$c = \frac{\int A_\parallel d\tilde{v}}{vN \int \varepsilon d\tilde{v} \, d_{e\parallel}} = \frac{\int A_\perp d\tilde{v}}{vN \int \varepsilon d\tilde{v} \, d_{e\perp}}, \text{ or} \qquad (29b)$$

for peak absorbances, or integrated absorbances (band areas), respectively. $\int \varepsilon d\tilde{v}$ is the integral molar absorption coefficient. Use of integrated absorbances is recommended in all cases, where band broadening or narrowing must be expected, *e.g.* due to conformational changes. v and N denote the number of equal functional groups per molecule, and the number of active internal reflections, respectively.

In the case of thin layers $(d<d_p, Fig. 2)$, it is often more adequate to use the surface concentration Γ instead of the molarity c. Γ is obtained from *Eqns. 29a, b* simply by multiplication by the layer thickness d.

$$\Gamma = cd \qquad (30)$$

3. Experimental Considerations

3.1. *Sensitivity Requirements for* **in situ** *Measurements*
Optimum Number of Internal Reflections

Considering the symmetric CH_2 stretching $(v_s(CH_2))$ band of a phospholipid monolayer, one should expect an absorptance of about 0.2% per internal reflection. From this point of view, 100 or even more internal reflections would be desirable. However, these mono and submonolayer absorptions have to be detected in aqueous environment which itself is a strongly absorbing medium (see *Fig. 5*). The latter requires as few internal reflections as possible. Optimization [46] resulted in $N = 20$–40 for a germanium IRE, and 10–20 for a ZnSe IRE (angle of incidence: $\Theta = 45°$).

3.2. *Significance of Liquid Water Compensation*

The vibrational spectrum of liquid water (see *Fig. 5* and [46]) is commonly the most intense part of the background to be compensated in IR spectroscopy of biological systems. Unfortunately, the amide-I band of peptides and proteins, which are sensitive to the secondary structure are completely overlapped by the H_2O bending $(\delta(H_2O): \sim 1640 \text{ cm}^{-1})$. In many papers published so far, access to amide I was performed by subtraction of the water background by means of the spectrometer software. Structural information was then obtained by application of *Fourier* self-deconvolution and/or curve-fitting techniques, to separate the amide-I band into components typical for secondary structural elements, such as α helix, pleated sheet, β turns, random. These results, however, are of little confidence, because bulk water and bound water exhibit different peak wavenumbers (up to 20 cm^{-1}) and different molar absorption coefficients (up to a factor of 10) [46]. As a consequence, one should be aware that bound water is an integral part of the sample. It cannot be subtracted, at least not by manual manipulations with a bulk water reference spectrum. For a more detailed discussion of this fundamental problem, see [46].

3.3. *ATR Attachment*
Single-Beam-Sample-Reference (SBSR) Technique

As a consequence of the required minimum number of internal reflections for monolayer spectroscopy on the one hand, and of the strongly absorbing background on the other hand, the spectral regions of OH stretching $(\sim 3400 \text{ cm}^{-1})$ and OD stretching $(\sim 2500 \text{ cm}^{-1})$ are completely blocked, depending on whether H_2O or D_2O is used as solvent. The transmittance

of the corresponding bending vibrations ($\delta(H_2O):\sim$ 1640 cm^{-1}; $\delta(D_2O):\sim$ 1200 cm^{-1}) is only a few percent under these conditions. A significant compensation of such strong bands is a prerequisite for *in situ* spectroscopy, and requires a good reproducibility of the optical path of the IR beam in the multiple internal-reflection element (MIRE), especially for corresponding sample and reference measurements. Moreover, a well-defined angle of incidence and number of internal reflections are important for quantitative analysis. We have achieved best results with dispersive [60][63–68] and *Fourier* transform (FT) instruments [46][61][62][105] by a single trapezoid MIRE (*Fig. 6*) for sample and reference, as well.

Using parallel incident light focused to the entrance face of the crystal by means of a cylindrical mirror, it was possible to place the sample, *e.g.* at the lower half, and the reference at the upper half of the MIRE. The IR beam is directed alternatively through sample and reference side. In dispersive instruments, a rotating chopper wheel with two rows of different numbers of holes (see *Fig. 7*) was used in order to label sample and reference beams with different frequencies.

Because sample and reference are measured with a single beam without cell displacement, this method is referred to as *Single-Beam-Sample-Reference* (SBSR) technique. The most obvious advantage of this attachment is the lack of problems with atmospheric H_2O and CO_2 absorptions. SBSR spectra exhibit also a better long-term stability than generally achieved in the single-beam mode [46]. Furthermore, SBSR technique enables *ad hoc* changes of the reference environment without problems, since there is no need for separate reference spectra which might require detachment of the ATR cell. The latter would be necessary in the single-beam (SB) mode, leading to a decrease of the accuracy of background compensation.

3.4. Modulation Spectroscopy
3.4.1. Introduction

A situation often encountered in chemical and biological IR spectroscopy is the detection of small structural differences on a molecular level, induced in a system by the change of external parameters, as the concentration of an agent, temperature, irradiation, electric field, *etc.* Conventionally, this information is obtained by measuring the IR spectra at two different parameter settings and then calculating the difference spectrum. The smaller this difference is, however, the more critical is the influence of system instabilities occurring between the two measurements.
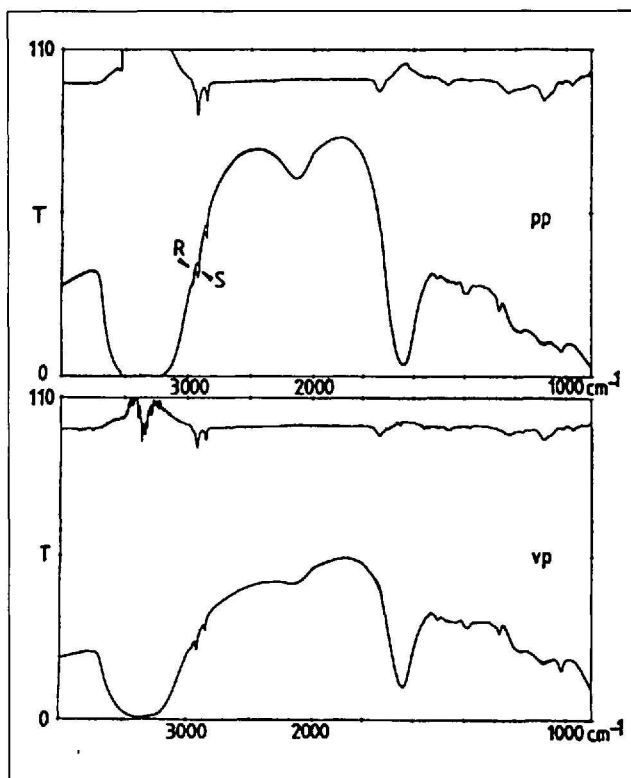

Fig. 5. *Polarized IR-ATR transmittance spectra of a palmitoyl-oleoyl-phosphatidylcholine (POPC) monolayer adsorbed tail/tail to a DPPA LB monolayer.* The polar head groups of POPC are in contact with aqueous buffer solution (100 mM NaCl, 20 mM phosphate, pH 7). Angle of incidence: $\theta = 45°$, number of active internal reflections: $N = 30$, temperature: $T = 20°$. Reference: DPPA LB-monolayer, same buffer. From [62].
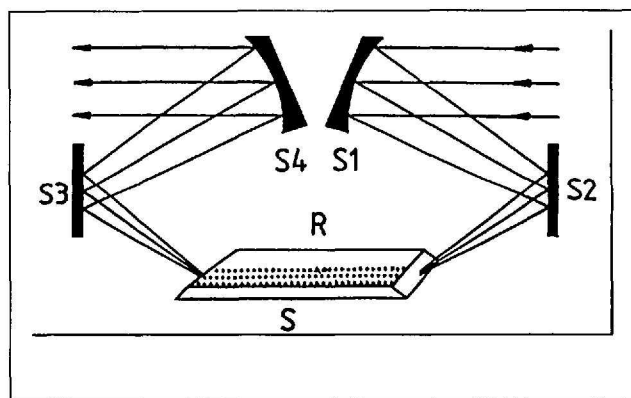

Fig. 6. *Single-Beam-Sample-Reference (SBSR) attachment.* The parallel incident beam is focused on the entrance face of a MIRE. The parallelism in the plate must be good to avoid crossing over between the sample (S) and reference (R) part. S1, S4: identical cylindrical mirrors. S2, S3: planar mirrors. The light is directed alternatively through the S and R side by means of a computer controlled chopper. From [62].

They decrease with decreasing time delay. SBSR technique, as described above, can reduce such instabilities considerably; however, best results are achieved in all cases in which modulation spectroscopy can be applied.

3.4.2. Requirements for the Applicability of Modulation Spectroscopy

The chemical or biological system to be investigated must allow a reversible or quasi-reversible periodic stimulation. If an external parameter is modulated by the circular frequency $\omega_m = 2\pi f_m$, all molecules of the sample which depend on this parameter will exhibit a concentration modulation of the same frequency, whereas all inert molecules remain unaffected. The use of phase-sensitive detectors (quadrature demodulation) enables a selective observation of the stimulated process in real time, whereas all inert components are suppressed (real time difference spectroscopy). Moreover, if the 'time constant' of the stimulated process is comparable to, or larger than the stimulation

period, a phase lag and a decrease of the amplitude will result, which both are typical for the kinetics of the process.

3.4.3. Theoretical Remarks

Consider a sample with concentration c, which may be influenced by a periodic modulation of an external parameter with circular frequency ω_m. The resulting concentration modulation may then be described by the *Fourier* series *Eqn. 31*:

$$c(t) = c_0 + 2c_1\sin(\omega_m t + \phi_1) + 2c_2\sin(2\omega_m t + \phi_2) + \ldots = c_0 [1 + \rho_1\sin(\omega_m t + \phi_1) + \rho_2\sin(2\omega_m t + \phi_2) + \ldots], \qquad (31)$$

where c_0 denotes the mean concentration (DC term) and $2c_k$ the corresponding *Fourier* coefficient of the $k \cdot \omega_m$ term. The degree of modulation is defined by

$$\rho_i = \frac{2c_i}{c_0} \quad (0 \le \rho_i \le 1) \qquad (32)$$

It should be noted that, if the stimulation is harmonic or rectangular, ρ_2 should only deviate from zero, if nonlinear reaction steps (other than first-order kinetics) occur in the chemical process.

According to *Lambert-Beer*'s law, the light intensity I_s after passing the sample S is given by

$$I_S = I_0 \cdot T_S = I_0 \cdot 10^{-\varepsilon c(t)d} = I_0 \cdot 10^{-A_s} \quad (33)$$

where T_S and A_S denote transmittance and aborbance of the sample. Introducing *Eqn. 31* into *33*, one obtains after reorganisation

$$I_S = I_0 \cdot T_{S0} \cdot T_{S1} \cdot T_{S2} \cdot \ldots \quad (34)$$

T_{Sk} ($k = 1,2,...$) denotes the transmittance corresponding to the modulated resposes of the frequency $k \cdot \omega_m$.

A typical experimental set-up which enables the mesurement of modulation amplitudes $\rho_k \varepsilon c_{S0}(\rho_k)d$, as well as the corresponding phase shifts ϕ_k with respect to the external stimulation is shown in *Fig. 7*. Both quantities, amplitude and phase shift, depend on the chemical reaction scheme and the rate constants. Therefore, reconstruction of a reaction scheme and determination of rate constants are possible by modulation spectroscopy at different stimulation frequencies ω_m [43][44][46].

4. Applications to Drug/Membrane Interaction Studies

4.1. *Preparation of Immobilized Bilayer Membranes*

Model membranes used for drug interaction studies are phospholipid bilayers immobilized at the surface of the MIRE (*Fig. 8*).For technical reasons, the preparation must be performed in two independent steps [62]. The first monolayer is transferred by means of the *Langmuir-Blodgett* technique [69]. The transfer from the air-water interface is achieved by withdrawing the ATR plate perpendicularly through the compressed monolayer at constant pressure and constant velocity (*Fig. 9*).

The monolayer coated dry plate is then mounted in a liquid sample cell which has been hydrodynamically optimized for flow-through experiments. For completion of the bilayer, a vesicular solution (1 mg of lipid/ml of buffer, sonication under N_2 flow at 35–40°) is circulated through the ATR cell (*Fig. 10*) resulting in spontaneous adsorption of phospholipid molecules.

The procedure was optimized based on electron micrographs (*F. Kopp et al.*, to be published) leading to very stable and reproducible lipid bilayer membranes. No lipid loss was detectable by pumping a buffer solution in a closed cycle during 12 h (1.9 ml/min). Recently, corresponding mixed POPC/POPG bilayers have been prepared for melittin interaction studies [27].

4.2. *Preparation of Double Bilayer Assemblies*

It was shown earlier [72][73] that membrane fragments with enriched Na,K-ATPase isolated from rabbit kidney adsorb spontaneously to black lipid membranes (BLM) of POPC. It turned out that these membrane fragments adsorb to a DPPA/POPC bilayer under the same conditions as they do to POPC BLM. The result is a double bilayer assembly as shown in *Fig. 8*. This procedure offers new possibilities for *in situ* studies with integral membrane
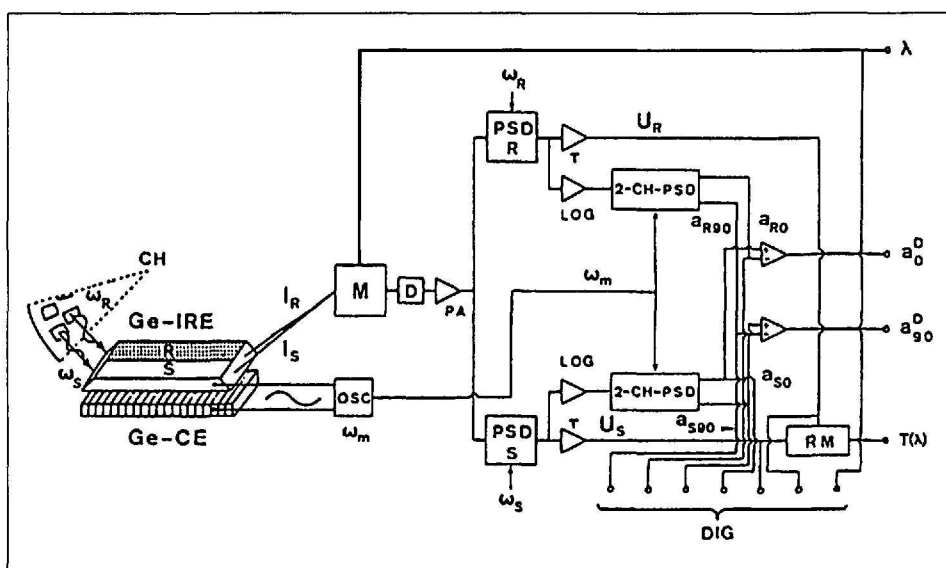

Fig. 7. *Schematic set-up of a dispersive IR-ATR (SBSR) modulation spectrometer for electric-field stimulation* [55][67][68]. CH: Chopper wheel with two rows of holes for modulation of incident light with circular frequencies ω_S (sample), and ω_R (reference); Ge-IRE: Ge internal reflection element with sample (S), and reference (R) area, see also *Fig. 6*. Ge-CE: Ge counter electrode for external electric-field stimulation with frequency ω_m by means of oscillator OSC. I_S, I_R intensities of sample, and reference beams, labelled by ω_S and ω_R. M: Monochromator. D: Detector. PA: Preamplifier. PSD: Phase-sensitive detectors for demodulation of carrier frequencies ω_S and ω_R. Stationary part. τ: low pass filters, the electrical dc components U_S and U_R are fed to a ratiometer (RM), resulting in the transmittance spectrum $T(\lambda)$ of the sample. *Dynamic part*. LOG: logarithmic amplifier. 2-CH-PSD: dual channel phase sensitive detector for the demodulation of externally stimulated $k\omega_m$ response ($k = 1,2,...$) of sample and reference ($a_{S0}, a_{S90}, a_{R0}, a_{R90}$) exhibiting 0° and 90° phase shift with respect to stimulation. a_0^D, a_{90}^D: differencies between corresponding 0° and 90° components of sample and reference. λ: wavelength. Relevant output signals are digitized (DIG) and stored in a computer.
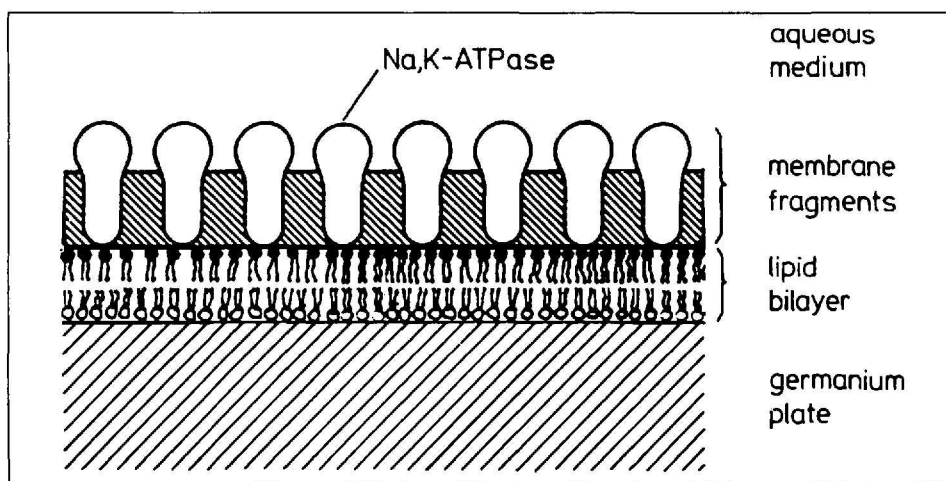

Fig. 8. *Internal-reflection plate covered with lipid and protein layers*. The Ge surface is initially coated with a phospholipid bilayer (see *Sect. 4.1*) and is in contact with aqueous solution. Replacing the aqueous solution is by a suspension of flat membrane fragments 0.2–1 μm in diameter containing oriented Na+/K+-ATPase molecules with a density of several thousand per μm², leads to binding of membrane fragments to the lipid bilayer. From [2].

proteins in their 'natural' lipid environment. For details, see [2].

4.3. *Immobilization of Membranes, Proteins and Living Cells*

For dissolved substances ATR, spectroscopy requires minimum concentration of $c_{min} \approx 1$–10 mM, depending on the molar absorption coefficient. The sensitivity is drastically enhanced upon immobilization of the sample at the MIRE/water interface. Two possibilities have been described in *Sect. 4.1* and *4.2*. A variety of applications such as adsorption of lipid membranes, adsorption or chemical immobilization of proteins as well as living cells (*e.g.* erythrocytes) are enabled by silanization of the surface of a germanium ATR plate [67][74]. Aminopropyltriethoxysilane has turned out to be optimum as silanizing agent.

4.4. *Interaction of Drugs with Model Membranes*

Local anesthetics (LA) of the tertiary amine type (procaine (I), oxybuprocaine (II), falicaine (III), and dibucaine (IV)) were used as model compounds to interact with lipid bilayers of the type described in *Sect. 4.1* (*Formulae* of LA).

All LAs were found to adsorb to the membrane. The higher the physiological activity of a given LA, the higher its affinity to condense to the DPPA/POPC bilayer, as well as to already adsorbed LA. Equilibrium surface concentrations have been determined and fitted by the *Brunauer-Emmett-Teller* (BET) isotherm (*Fig. 11*) [75].

From molecular-model considerations, one may estimate the maximum and minimum monolayer concentration of oxybuprocaine to be $\Gamma_{max} = 4.15 \cdot 10^{-6}$ mol/m^2 and $\Gamma_{min} = 1.38 \cdot 10^{-6}$ mol/m^2, respectively. Therefore, one has to conclude LA-multilayer condensation even at clinical application concentations (5–100 mM). More recent interaction studies of dibucaine (DIBU) with DPPA/POPC and DPPA/DMPC bilayers [61] have confirmed this finding. For these studies DIBU was dissolved (0.5–10 mM) in aqueous solutions of 100 mM NaCl at pH 5.5 (borate-phosphate-citrate buffer, 20 mM) for DPPA/POPC membranes, and at pH 6.7 (phosphate buffer, 20 mM) with DPPA/DMPC-d$_{54}$ membranes. The volume of the ATR cell was 250 μl. To establish constant bulk concentration in the sample ATR cell, 5–10 ml of DIBU solution was permanently cirulated in a closed cycle, (*Fig. 10*). *Fig. 12* shows typical polarized spectra of 10 mM DIBU in contact with a DPPA/POPC membrane (trace *a*). A corresponding membrane buffer solution was in the reference (*R*) ATR cell, (see *Fig. 6*).
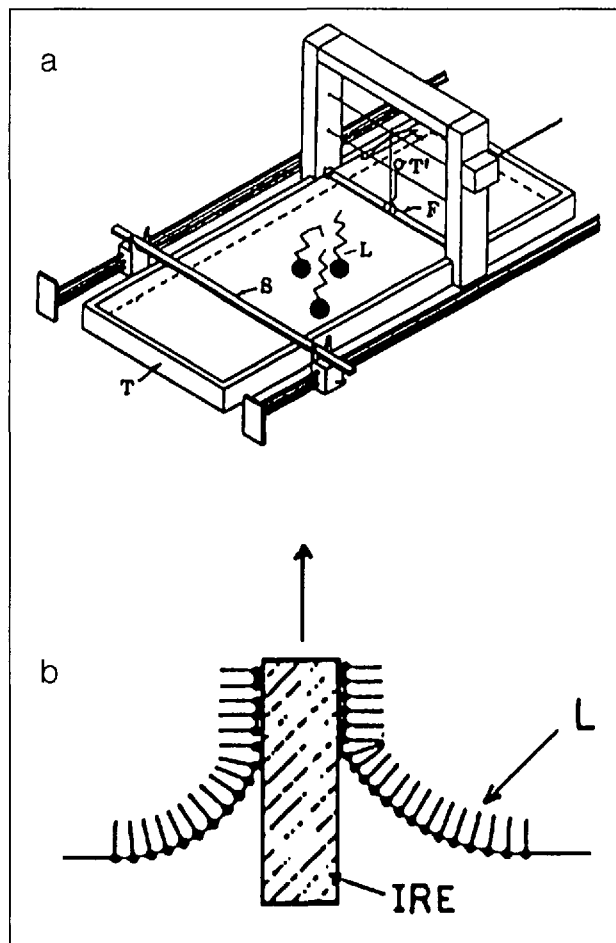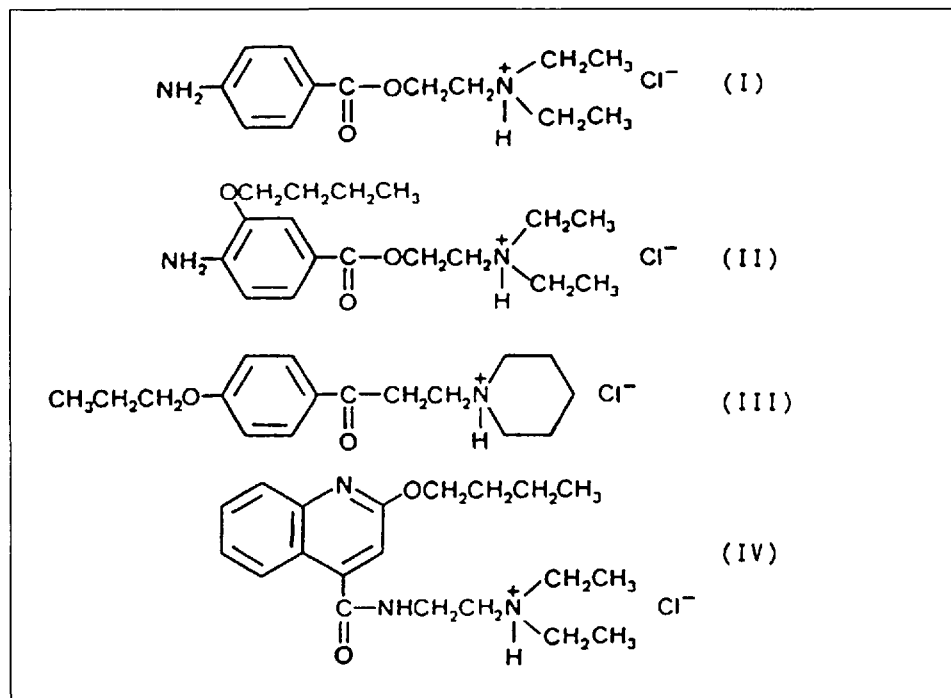
Fig. 9. a) *Film balance. T*, trough filled with aqueous subphase; S, sweep for compression of lipid monolayer (L) spread at the air-water interface; F, float connected to torsion wire (T') for film pressure measurement. b) *Transfer of a compressed lipid monolayer from the air-water interface to a solid substrate (MIRE) by the* Langmuir-Blodgett *technique, see* [69–70].

Trace *a* of *Fig. 12* reveals, therefore, membrane-bound and bulk DIBU, as well as DIBU-induced structural changes of the membrane. For comparison, corresponding spectra of 100-mM bulk DIBU were scaled (×0.37) to about the same intensity (trace *b*). Both experiments were performed at rather non-physiological pH 5.5 in order to enable direct comparison with published NMR data [76–79]. The fact

that the absorbance spectrum of 100-mM bulk DIBU has to be scaled by 0.37 instead of 0.10 in order to match the absorbance of 10-mM DIBU interacting with the membrane, reveals unambiguously that about 2/3 of the absorbance of DIBU results from membrane bound LA. Quantitative analysis by *Eqns. 8, 9*, and *25–30* results in a surface concentration of total DIBU (LA$_{tot}$) of $7.8 \cdot 10^{-6} \pm 0.4 \cdot 10^{-6}$ mol/m^2.
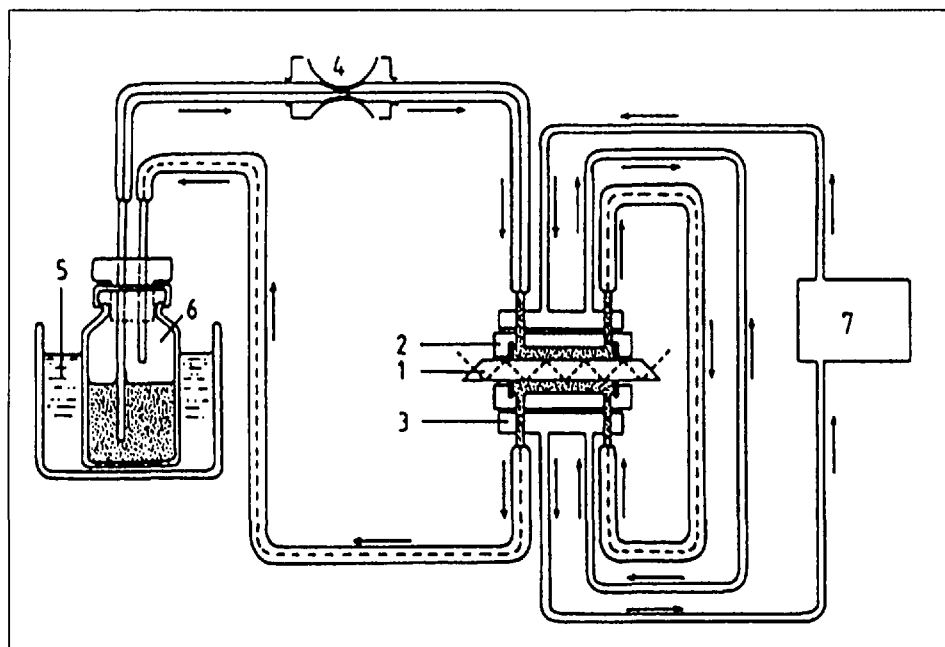
Fig. 10. *Schematic set-up for IR-ATR* in situ *experiments. 1:* Multiple internal reflection element (MIRE, ATR plate), *e.g.* with immobilized membrane; *2:* liquid sample cell for flow-through and stationary experiments; *3:* thermostat; *4:* pump; *5:* thermostat for substrate reservoir; *6:* substrate reservoir; *7:* MIRE thermostat. From [71].
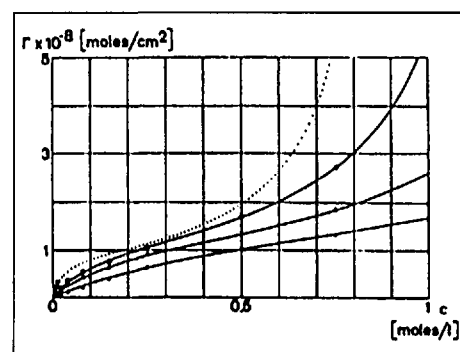

Fig. 11. *Adsorption isotherms of procaine (•), lower trace, oxybuprocaine (Δ), falicaine (*), and dibucaine (o), upper trace.* 20 mM phosphate buffer, pD 7.0, 100 mM NaCl. Note, that increasing physiological LA activity is reflected by the increasing adsorption tendency. From [75].

Assuming a cross-section of 45–67 Å² per molecule [77], one obtains 2–3 DIBU monolayers bound to the DPPA/POPC membrane at 10-mM bulk concentration. In contrast, *Seelig et al.* [77], reported still sub-monolayer coverage at the same bulk
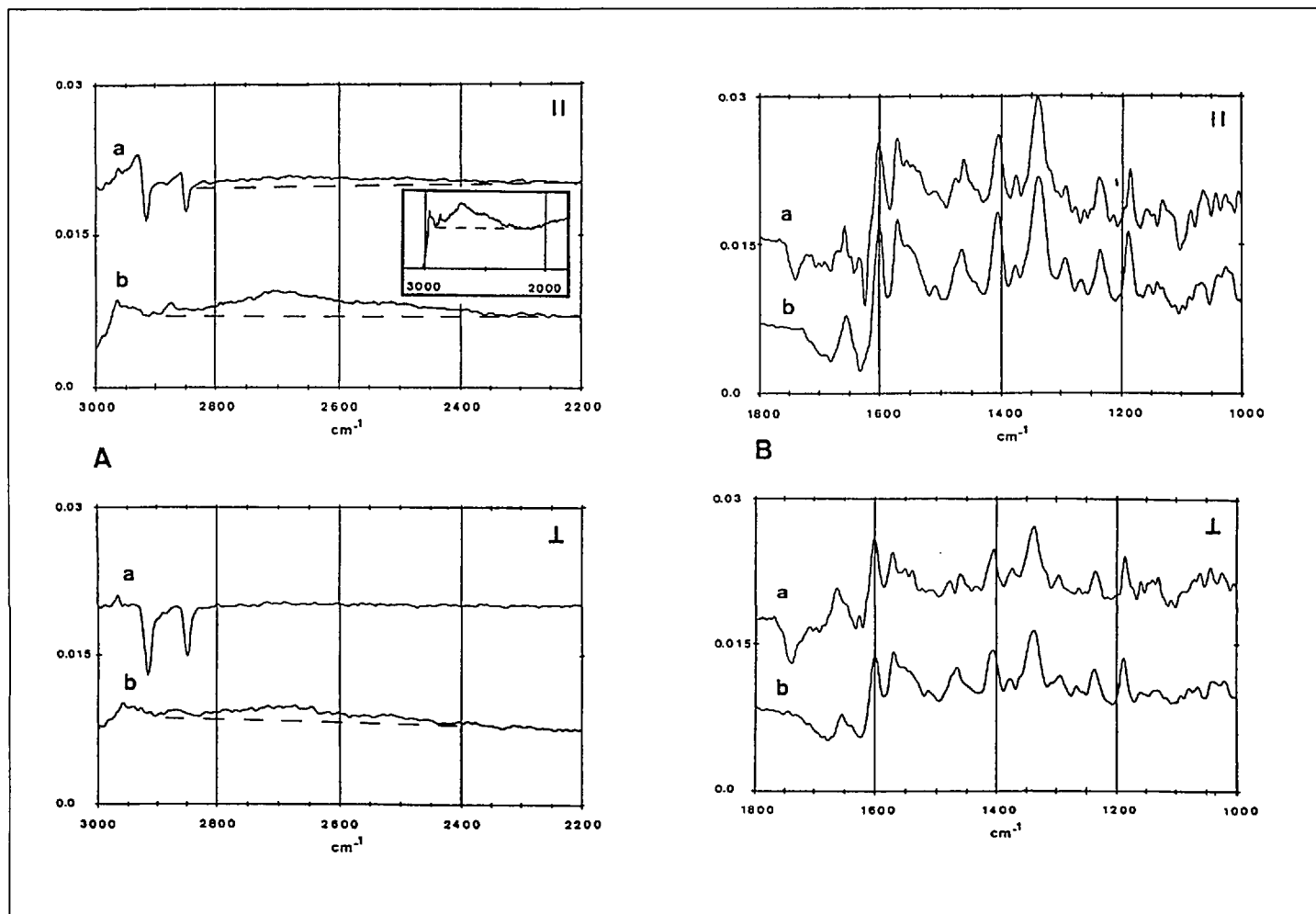

Fig. 12. *Polarized IR-ATR absorbance spectra of a 10-*mM *dibucaine (DIBU) solution* (100 mM NaCl, 20 mM borate-phosphate-citrate (BPC) buffer, pH 5.5) *interacting with a DPPA/POPC bilayer membrane* (trace a), *and for comparison, 100-*mM *DIBU solution in contact with the pure* Ge *ATR plate* (trace b), *scaled with 0.37 in order to get approximately the same band intensities* (same buffer). Insert: Compressed wavenumber scale of the latter in the υ(NH⁺) region (same absorbance scale). Angle of incidence: θ = 45°, number of active internal reflections: N = 19, temperature: T = 25°. Reference: DPPA/POPC bilayer (see *Sect. 4.1*), same buffer. Wavenumber range: 3000–2200 cm⁻¹ (A), 1800–1000 cm⁻¹ (B). *Note. i)* Only *ca.* 1/3 of the DIBU absorbance (trace a) results form dissolved DIBU. 2/3 is bound DIBU as a consequence of the scaling factor 0.37 for the trace b spectrum. Calculated surface concentration: Γ = (7.8 ± 0 4) 10⁻⁶ mol m⁻². *ii)* Dissolved DIBU is protonated (pK_a = 8.83). Membrane-bound DIBU appears partly as base, as concluded from corresponding υ(NH⁺) absorbance near 2700 cm⁻¹. *iii)* The unusual behaviour of typical lipid bands (υ(CH), υ(C=O), υ(C–O), υ(POC)) is reversible and does not reflect lipid loss, see text.

DIBU concentration and pH. One reason for the discrepancy results probably from different bilayers. Symmetric POPC multilayers were used in [77]. In our case, also POPC was faceing the aqueous environment (DIBU), however, the counter monolayer, faceing the Ge-ATR plate, was Ca++- DPPA. Although the DPPA polar region is not directly accessible by DIBU (*Fig. 8*), the resulting negative trans-membrane electric field could facilitate DIBU binding and incorporation into the membrane. A second reason could be of systematic nature, since the experimental approaches are quite different (see *Sect. 4.5*).

Concerning the lipid response to DIBU binding, there is evidence for a reorientation of the choline head group (negative band at 1491 cm^{-1} [45]) in agreement with [77][80]. More significant lipid responses, however, result from ν(CH$_2$): 2800–3000 cm^{-1}, ν(CD$_2$): 2000–2300 cm^{-1}, ν(C=O): ~1740 cm^{-1}, δ(CH$_2$): 1470 cm^{-1}, ν(C–O): ~1180 cm^{-1}, v_s(PO$_2^-$) and for v_{as}(PO$_3^-$): ~1100 cm^{-1}, v_s(PO$_3^-$): ~1000 cm^{-1}.

Since the reference to the spectra shown in *Figs. 12* and *13* are the corresponding bilayer membranes and buffer solutions the negative responses of lipid bands could indicate material loss upon LA interaction. This, however, is not the case, because the effects are reversible after LA replacement by buffer [61].

A similar, also less pronounced behaviour was also observed earlier with the LA oxybuprocaine [62]. LA-induced conformational changes in the hydrocarbon chain, fatty-acid ester, phosphate, and choline regions have to be concluded. Hydrocarbon-chain disordering is also indicated by broadening and upwards shifts of $v_{as,s}$(CH$_2$) and $v_{as,s}$(CD$_2$) [61]. Both phenomena are qualitative features for the formation of gauche defects [81]. Quantitative analysis is possible *via* the dichroic ratio dependence of $v_{as,s}$(CH$_2$) on bulk DIBU concentration (*Fig. 14*), or by dichroic analysis of the difference bands (*Figs. 12* and *13*). Concerning the former, *Fig. 14* shows the dependence of the mean dichroic ratio of v_{as}(CH$_2$) and v_s(CH$_2$) of a DPPA/POPC membrane interacting with DIBU (S) at pH 5.5 and with buffer (R).

Since data were collected in the SBSR mode (see Fig. 6) the age of both membranes, S and R, was exactly the same. The ν(CH$_2$) dichroic ratio of the R membrane remained constant over the whole duration of the experiment. Maximum dichroic ratio (1.37 ± 0.04) is reached at *ca*. 3-mM bulk concentration, indicating saturation of the effect. This could mean that maximum chain disordering is reached. Since 3-mM bulk DIBU correspond to more than a monolayer adsorbed DIBU [61], and
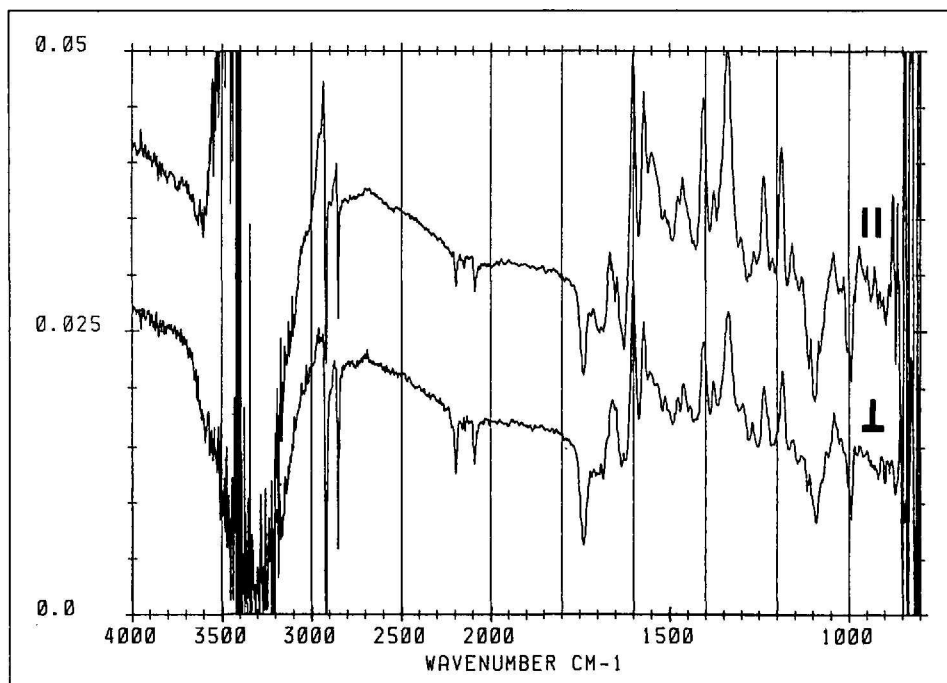

Fig. 13. *Polarized IR-ATR absorbance spectra of a 10-mM dibucaine (DIBU) solution* (100 mM NaCl, 20 mM phosphate, pH 6.7) *interacting with a DPPA/DMPC-d$_{54}$ bilayer membrane.* Angle of incidence: θ= 45°, number of active internal reflections: N = 26, temperature: T = 25°. Reference: DPPA/DMPC-d$_{54}$ in contact with the same buffer. *Note.* The response of the hydrocarbon chains υ(CH): 2800–3000 cm^{-1}, υ(CD): 2100–2300 cm^{-1}, the fatty acid ester groups υ (C=O): 1740 cm^{-1}, υ(C–O): 1180 cm^{-1}, and v_s(PO$_2^-$), v_{as}(PO$_3^-$): 1100 cm^{-1}, v_s(PO$_3^-$): 1000 cm^{-1}.
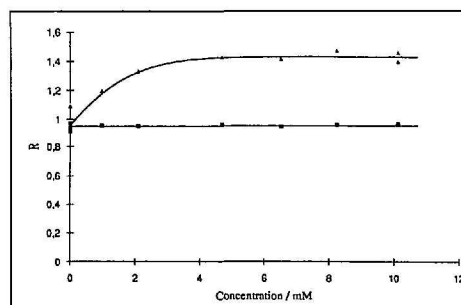

Fig. 14. *Dependence of the mean dichroic ratio of symmetric and antisymmetric CH$_2$ stretching of a DPPA/POPC bilayer on bulk DIBU concentration.* 100 mM NaCl, BPC buffer pH 5.5, 25°. S: Sample, 0–10 mM DIBU. R: Reference, same as S except without DIBU.

since an isotropic layer would have a dichroic ratio of R_{iso} = 1.75 ± 0.05, it rather tends to the interpretation, that DIBU coats the membrane, thus, preventing further disordering. On removing the 10-mM DIBU solution, a certain hydrocarbon-chain disordering is restored, although no remaining DIBU could be detected in the membrane. These data, and the directly measured difference spectra (*Figs. 12*, and *13*) enable the determination $\Sigma_{i,k} \sigma^S_{i,k}, \Sigma_{i,k} \sigma^R_{i,k}$, and $\Sigma_{i,k} (\sigma^S_{i,k} - \sigma^R_{i,k})$, respectively. $\sigma_{i,k}$ denotes the orientation function (*Eqn. 21*) of the k-th CH$_2$ group in the i-th chain (i = 1.2) (to be published). Preliminary simulations by *Eqn. 23* reveal that the magnitude of the change of dichroic ratios under the influence of DIBU (*Fig. 14*) as well as the prominent ν(CH$_2$) response (*Fig. 13*) requires disordering of the hydrocarbon

chains of the inner DPPA monolayer, too. The preliminary assignment of the difference band at 1000 cm^{-1} (*Fig. 13*) to v_s(PO$_3^-$) gives some evidence for DIBU permeation across the membrane.

Unambiguous information on conformation and orientation of bound DIBU would only be available from partly isotopic labelled LA, *e.g.* ^{18}O and ^{2}H in oxybutyl, ^{15}N selectively in the aromatic ring, amide, and ammonium group. Nevertheless, a preliminary analysis of actual data is given in [61].

4.5. Drug-Membrane Part*ition Coefficient*

Since the volume of a bilayer membrane is small and in some cases may become comparable to that of bound drug, it is reasonable to define the apparent partition coefficient by

$$P_{app} = \lim_{c_b \to 0} \frac{c_m}{c_b} \qquad (35)$$

where c_m and c_b denote the drug concentrations in the membrane and in the bulk [82]. A number of different methods for partition coefficent determination have been applied so far. The most common one is equilibration of the drug with lipid vesicles, followed by centrifugation and determination of the drug in the supernatant by optical methods. The membrane bound amount is then calculated by *via* mass conservation. Pellets are often used for further investigations by NMR or ESR
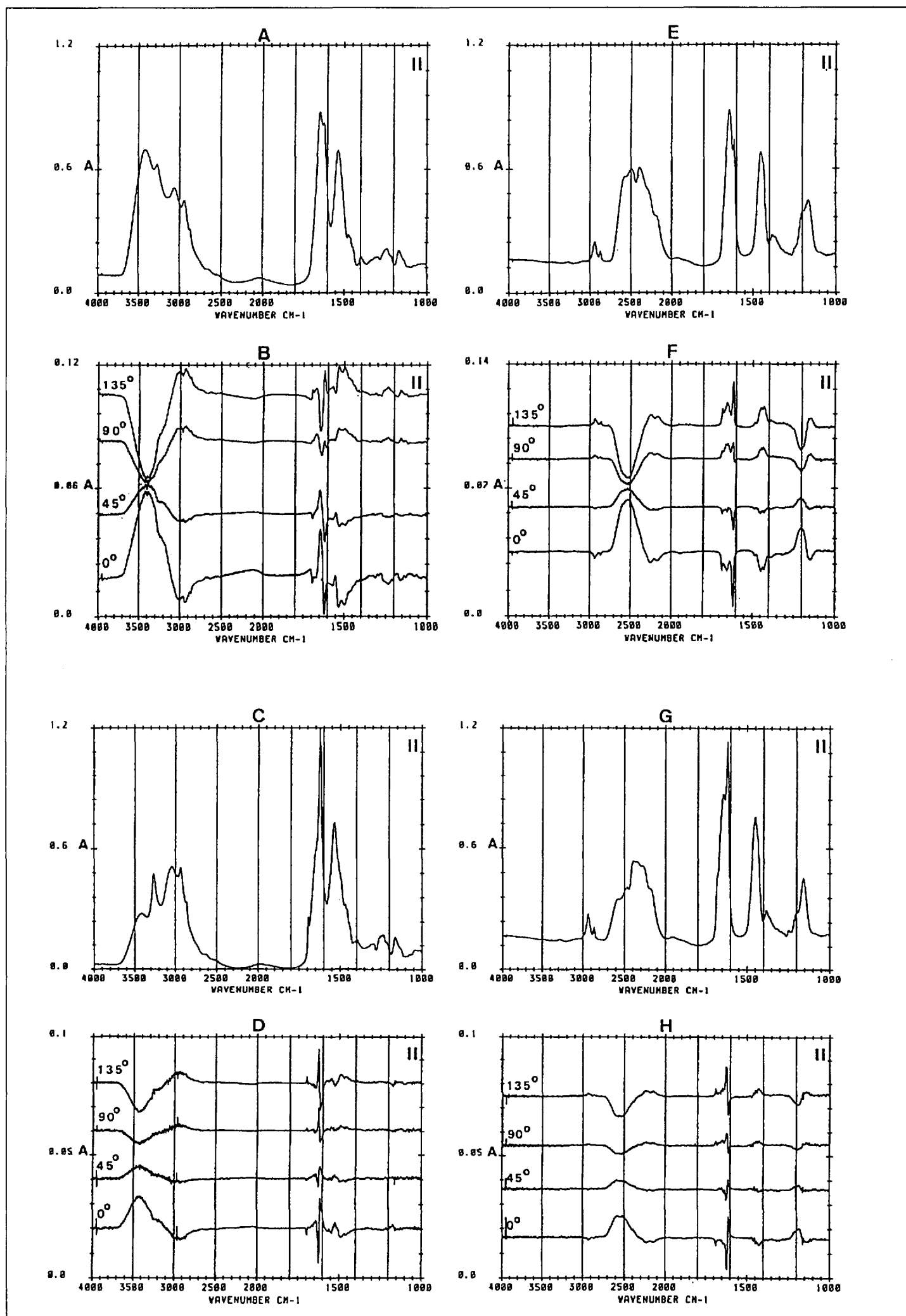
Fig. 15. *Stationary and temperature (T) modulated FTIR ATR spectra of hydrated poly(L-lysine) multilayers on a Ge ATR plate (MIRE)*. Environment: $\approx$ 90% rel. humidity H_2O (A–D) and D_2O (E–H). Mean temperatures: T = 26° (A,B,E,F) and T = 35° (C,D,G,H). *Stationary spectra*: Predominant antiparallel β structure (pleated sheet) at 35° (1625/1695 cm^{-1}, C, and 1618/1692 cm^{-1}, G). More complex conformational equilibrium at 26°, α-helix and/or random (1655 cm^{-1}, A, 1643 cm^{-1}, E) in equilibrium with antiparallel β structure. Amide I band in H_2O environment overlapped by $\delta(H_2O)$ (~1640 cm^{-1}, A,C). Complete H/D-exchange in D_2O environment (E,G, v(NH): ~ 3300 cm^{-1}, v(ND): ~ 2400 cm^{-1}, amide II: ~ 1540 cm^{-1}, amide II': ~ 1450 cm^{-1}). T-modulation spectra: amplitude: ΔT = ± 1.5° (B,F), ΔT = ± 1.0° (D,H). Period: τ_m = 11 min (*i.e.* 5.5 min T–ΔT and 5.5 min T+ΔT). Phase shift with respect to stimulation: 0° (lower trace), 45°, 90°, 135° (upper trace). Modulation bands of H_2O (~ 3400 cm^{-1}, ~1640 cm^{-1}) and D_2O (~2500 cm^{-1}, ~ 1200 cm^{-1}) result from temperature- and conformation-induced hydration changes, therefore, amide I (~1650 cm^{-1}) analysis is more relevant in D_2O environment (F,H). Modulation at T = 35° stimulates a transition (1625/1619 cm^{-1}, D, 1620/1616 cm^{-1}, H) probably between two β structures. This transition occurs at T = 26°, too (90°-phase shift, 3rd trace from bottom, B,F). However, α helices and/or random structures are also involved (~ 1655 cm^{-1}) The complexity of the transition is reflected by the phase dependent shapes of the amide I,I' bands, which is typical for multistep reactions. Angle of incidence: 45°, number of active internal reflections: N = 26. Reference for stationary spectra: Clean MIRE.
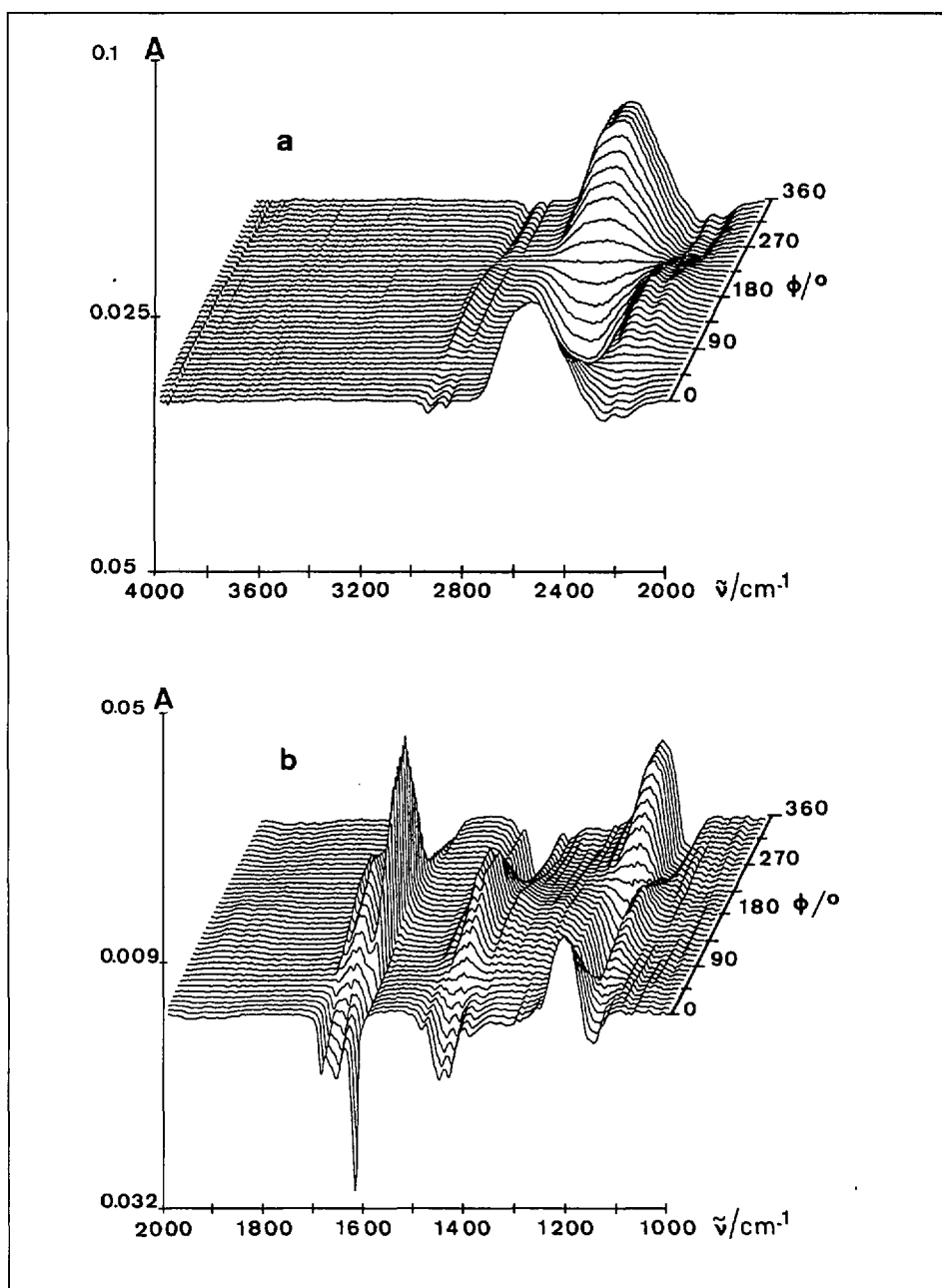
[76–79][83–86]. Other methods are based on dialization [87], freezing-point depression [88][89], and electrophoretic mobility (ζ-potential) measurements [83][90]. Since many drugs may assume a charged and uncharged state (amines, carboxylic acids) depending on the environment, it is reasonable to take electrostatic effects into account for the discussion of membrane partitioning. Most of these approaches are based on the *Gouy-Chapman* model [77][83][88][91–94]. There is general agreement that tertiary amines (*e.g.* LAs) undergo an apparent pK_a decrease of ΔpK_a $\approx$ 1.5 upon membrane binding. Membrane bound LAs with a bulk pK_a between 8 and 9 may, therefore, be expected predominantely in the protonated state at bulk pH 5.5 [76–79], which is in contrast to our finding, see below.

Although these methods are generally applied, there is still room for some critical remarks. Firstly, concerning the centifugation approach: to get a supernatent free of lipids, up 300 000 g are applied for 1–3 h. This leads probably to an equilibrium between drug in the supernatant, in the interlamellar water phase (the pellet consists of multibilayers), and in the mem-

Fig. 16. *Temperature-(T) modulated FTIR ATR spectra of D_2O hydrated poly(L-lysine) multilayers*. The spectra result from the same experiment as described in the legend to *Fig. 15F*. Phase resolution 9°. Phase delay with respect to T stimulation: 0° first spectrum (foreground), 351° last spectrum. *a)* 4000–2000 cm^{-1}, *b)* 2000–1000 cm^{-1}.

brane. One may ask, whether this system at the moment of separation of supernatant and pellet still represents the equilibrium state before centrifugation? From the thermodynamic point of view, it is not only a question of high-pressure application, but also of activity alteration in the interbilayer water phase. Secondly, many questions arise with respect to the electrostatic approach: is the *Gouy-Chapman* model adequate to describe the inhomogeneous surface potential profile resulting from single adsorbed charges? In this respect, an alternative approach has been given by *Ninham* and *Parsegian* [95] taking account of the local potential of membrane-bound charged species. Furthermore, can counter-ion binding be neglected as in most applications cited above? Why is the

interfacial and bulk permittivity set to be equal, although considerable differences have to be expected [96]? This has influence on the *Boltzmann* distribution of ions between bulk and interface and results in a *Born* energy term. Concerning ζ-potential measurements, there are also uncertainties with respect to non-uniform vesicle population, distance of the plane of shear from the vesicle surface (generally assumed to d_ζ= 2 Å). Alteration of surface structure by the adsorption of charged molecules may also influence d_ζ.

Finally, adsorption of charged particles leads to a surface potential, which will induce compensating reactions such as counter-ion adsorption and dissociation or association of H^+ (pK_a shift). Structural alterations may occur, too.

One should be aware, that in cited applications many 'hidden' parameters had to be estimated in order to enable a quantitative analysis of experimental data. The need for complementary experimental techniques with direct access to the quantities of interest is obvious. In this respect, IR ATR spectroscopy is a promising approach. Typically, the drug solution is circulated through the sample cell (see *Figs. 6* and *10*). Therefore, there is no ambiguity with respect to the bulk concentration. If necessary, it can be monitored on line. On the other hand, drug binding is detected simultaneously *in situ via* ATR. Quantitative analysis is straightforward as described in *Sect. 2*.

Concerning DIBU binding to a DPPA/POPC membrane, we have measured the adsorption isotherms for both, total DIBU (LA_{tot}) using the aromatic ring vibration at $1407 cm^{-1}$, and protonated species (LAH^+) by means of the $N-H^+$ stretching vibration at $2700 cm^{-1}$ [61]. It follows that, already at bulk DIBU concentration of *ca.* 1mM, the bound total amount of DIBU is sufficient to form a compact monolayer. However, the bound protonated species LAH^+ reaches this limit only at 2–6-mM bulk concentration, although there is 99.96% LAH^+ and only 0.04% LA at pH 5.5 in the bulk environment ($pK = 8.83$). Furthermore, about one half of bound DIBU is deprotonated and exists as base (LA) even at bulk pH 5.5. This ratio of charged to uncharged DIBU is also maintained in the DIBU multilayer region at ≥ 5 mM bulk concentration. Note that *Fig. 12* gives already evidence for significant DIBU deprotonation upon binding to the membrane. It should be mentioned that the bulk concentration of LA and LAH^+ are known and maintained constant during the adsorption process by using a closed cycle flow-through system (*Fig. 10*) with a large buffered substance reservoir. The adsorption isotherms of LAH^+ and (LA_{tot}) fit well to the simple *Langmuir* isotherm $\Gamma = c_b B/(a+c_b)$. *B* and *a* denote the monolayer surface concentration, and the ratio of desorption/adsorption rate constants. The concentration of a compound in the membrane c_m is related to the experimentally accessible surface concentration Γ by $c_m = \Gamma/d_o$, where d_o denotes the membrane thickness ($d_o = 5$ nm). According to *Eqn. 35*, the apparent partition coefficient may be expressed by the *Langmuir* parameters and the membrane thickness

$$P_{app} = \frac{B}{a\, d_o} \tag{36}$$

The resulting partition coefficients are found to be $P_{app}(LA_{tot}) = 1060 \pm 86$,

$P_{app}(LAH^+) = 475 \pm 93$, and $P_{app}(LA) = 9.99 \cdot 10^5 \pm 1.87 \cdot 10^5$, all data with 95% confidence limits [61]. The values for the total amount LA_{tot} and for LAH^+ are experimental, whereas values for the base LA are calculated from the difference of the surface concentrations of LA_{tot} and LAH^+. The *Langmuir* parameters B and a lose their original meaning and have to be considered as fitting parameters for an experimental isotherm, since electrostatic interactions as well as surface reactions ($LAH^+ \rightarrow LA + H^+$) and multilayer adsorption occur. In view of the finding that considerable amounts of DIBU base exist, probably in the hydrophobic region of the membrane, electrostatic approachs on the basis of the assumption that every bound DIBU carries a positive charge to the membrane surface are not reasonable, even at bulk pH = 5.5. An interfacial pK_a shift of *ca.* –1.5 units may still be true (although there is poor experimental substanciation, see above), since DIBU base can escape from the interface into more hydrophobic membrane regions. Ellipsometry could give valuable additional information on membrane thickness during the adsorption process, as well as on surface roughness and optical constants.

4.6. *Modulation Spectroscopy*

Modulation spectroscopy is a very sensitive and selective technique for the detection of weak periodic changes of the state of a sample induced by an external periodic change of any thermodynamic parameter. Moreover, detailed kinetic information is available, too. Modulation techniques have a wide field of applications [97] (see also *Sect. 3.4*) because of considerable signal/noise (S/N) enhancement with respect to stationary procedures. In our case, we estimate a S/N enhancement by a factor of about 10.

Polarization modulation (~ 50 kHz) was the first application with FTIR instruments [98]. This method, however, is of minor importance in bio FTIR spectroscopy. In conjunction with ATR it is even inadequate because of different effective thicknesses for ‖-, and ⊥-polarized incident light, (see *Eqns. 8–10*), and ‘Dichrioic Difference Spectra’ (*Sect. 2.3.5*).

Here, we report the first FTIR modulation spectra at low stimulation frequency [99]. Temperature (*T*) modulation of hydrated poly(*L*-lysine) was used, because it exhibits a conformational equilibrium which is very sensitive to hydration and *T* changes as well as to pH changes [100–105]. *T*-modulation experiments have been performed with hydrated (H_2O and D_2O ~ 90% rel. humidity at 20°) multilayers of poly(*L*-lysine) at 26° and 35° mean temperature, respectively. The modulation

amplitudes were $\Delta T = \pm (1.0 - 1.5°)$, with a period $\tau_m = 11$ min. The spectra shown in *Fig. 15* demonstrate the considerable potential of modulation spectroscopy in resolving small differences and enabling access to complex kinetics. A detailed analysis will be given elsewhere [105]; however, some obvious features should be mentioned here (see also legend to *Fig. 15*). *Fig. 15 A* and *E* present the stationary part of the spectra at 26° hydrated by H_2O and D_2O, respectively. *Fig. 15 C* and *G* show the corresponding spectra at 35°. Evidently, a conformational equilibrium (antiparallel pleated sheet with α-helix and/or random) exists at 26°, whereas antiparallel pleated sheet conformation dominates at 35°. The former state is optimum for modulation experiments, since the temperature induced change of an equilibrium constant K,

$$\frac{d\ln K}{dT} = \frac{\Delta H}{RT^2} \tag{37}$$

is most efficient with respect to changes in the equilibrium concentrations. ΔH denotes the standard enthalpy of reaction and R the gas constant. Sign and magnitude of ΔH of each elementary step as well as the corresponding rate constants determine the degree of modulation ρ_i and the phase angle ϕ_i (see *Eqns. 31–34*). As a consequence, phase-resolved spectra at a given modulation frequency $\omega_m = 2\pi/\tau_m$ and the dependence of the degree of modulation ρ_i and phase angle ϕ_i on ω_m give detailed insight in the number and sequence of species affected by external stimulation [43][44][105]. Modulation spectra (*Figs. 15B,D,F,H*) are resolved at 0°, 45°, 90°, and 135° phase shift with respect to the onset of *T* stimulation. For better understanding, it should be noted that a positive band in the 0°-spectrum generally means formation, and a negative band disappearance of a species upon stimulation. Typical H_2O and D_2O bands (~ 3400, ~ 1640 cm^{-1} (H_2O), ~ 2500, ~ 1200 cm^{-1} (D_2O)) have positive signs. Consequently, water binding from the atmosphere (N_2/H_2O, D_2O, ~ 90% rel. humidity at 20°) is enhanced by *T*-stimulation. This is reasonable, since the stimulation cycle started at minimum temperature $T - \Delta T$ followed by an increase to the maximum temperature $T + \Delta T$. Pleated sheet bands have opposite sign, indicating that the conformation is favoured at elevated temperature. Furthermore, it should be mentioned that a modulation band reaching maximum amplitude at phase angle $\phi = \phi_i$, is erased at $\phi = \phi_i \pm 90°$. Therefore, if in a composed band *e.g.* amide I, I (~ 1650 cm^{-1}), amide II' (~ 1540 cm^{-1}), amide II (

~ 1450 cm⁻¹) the components respond with different kinetics to the external stimulation, the shape of the overall band should depend on the reference phase angle (here: 0°, 45°, 90°, 135°). This is indeed the case in the spectra presented in *Fig. 15*, documenting that phase resolved spectra may give a detailed und unambiguous insight into complex bands. Working with a phase resolution of 9° enables data presentation in a 3D plot (*Fig. 16*). The experimental data are the same as used in *Fig. 15F*. It should be noted that all absorption bands of a given species must exhibit the same phase angle, *i.e.* if a maximum of a modulation band appears at a different phase angle, it unambiguously results from a different species.

5. Prospects

This review article has featured general and special aspects of IR ATR spectroscopy. Results justify the hopes that this technique may become a serious complement in drug design and drug delivery. Of course, there is need for further refinements of experimental methods and theory. In this context, it is planed to introduce more general ultrastructural models adequate for dichroic analysis of oriented poly- and oligopeptides, as well as of hydrocarbon chains. For that purpose, it is essential to get informations on energetically reasonable local conformations, *i.e.* on local distibution functions. Such data are available from molecular modeling. On the other hand, data on molecular structure derived from IR ATR can be used to filter the variety of possible structures derived from molecular modeling. Such concerted investigations are not limitted to immobilized oriented samples. Molecular structures can be studied in solution, too, provided the concentration of the solute is greater than 1–10 mM, depending on the molar absorption coefficients. Especially external parameter modulation techniques will be applied in a variety of different forms enabling the detection and analysis of conformational equilibria in immobilized and dissolved samples.

[1] P.R. Griffiths, 'Chemical Infrared Fourier Transform Spectroscopy', John Wiley and Sons, Inc., New York, 1975.

[2] U.P. Fringeli, H.-J. Apell, M. Fringeli, P. Läuger, *Biochim. Biophys. Acta* **1989**, *984*, 301.

[3] K. Brandenburg, U. Seydel, *Eur. J. Biochem.* **1988**, *16*, 83.

[4] M.S. Braimann, K.J. Rothschild, *Eur. J. Biochem.* **1988**, *17*, 541.

[5] U.M. Ganter, W. Gärtner, F. Siebert, *Eur. Biophys. J.* **1990**, *16*, 295.

[6] A. Barth, W. Kreutz, W. Mäntele, *Biochim. Biophys. Acta* **1991**, *1057*, 115.

[7] A. Blume, W. Hübner, G. Messner, *Biochemistry* **1988**, *27*, 8239.

[8] T.I. Lotta, I.S. Salonen, J.A. Virtanen, K.K. Ecklund, P.K.J. Kinnunen, *Biochemistry* **1988**, *27*, 8158.

[9] F. Tanfani, A. Ambrosini, G. Albertini, E. Bertolini, G. Curatola, G. Zolese, *Chem. Phys. Lipids* **1990**, *55*, 179.

[10] H.J. Casal, R.L. McElhaney, *Biochemistry* **1990**, *29*, 5423 .

[11] W.K. Surewicz, H.H. Mantsch, *Biochim. Biophys. Acta* **1988**, *952*, 115.

[12] H.-U. Gremlich, U.P. Fringeli, R. Schwyzer, *Biochemistry* **1984**, *23*, 1808.

[13] P.L. Poole, D.J. Barlow, *Biopolymers* **1986**, *25*, 317.

[14] P.I. Haris, D. Chapman, R.A. Harrison, K.F. Smith, S.J. Perkins, *Biochemistry* **1990**, *29*, 1377.

[15] F. Kopp, U.P. Fringeli, K. Mühlethaler, Hs.H. Günthard, *Biophys. Struct. Mech.* **1975**, *1*, 75.

[16] R.M. Gendreau, *Trends Anal. Chem.* **1986**, *5*, 68.

[17] R.J. Jakobsen, F.M. Wasacz, K.B. Smith, 'Chemical, Biological and Industrial Applications of Infrared Spectroscopy', Ed. J.R. Durig, John Wiley & Sons, New York, 1985, p. 199.

[18] E. Goormaghtigh, R. Brasseur, P. Huarz, J.M. Ruysschaert, *Biochemistry* **1987**, *26*, 1789.

[19] A. Mellier, 'Spectroscopy of Biological Molecules, New. Advances' Eds. Schmid, Schneider, and Siebert, J. Wiley, Chichester, 1988, p. 173.

[20] J.L.R. Arrondo, A. Muga, J. Castresana, C. Bernabeu, F.M. Goni, *FEBS Lett.* **1989**, *252*, 118.

[21] J. Villalain, A. Ortiz, J.C. Gomez-Fernandez, *Biochim. Biophys. Acta* **1988**, *941*, 55.

[22] D.G. Cornell, R.A. Dluhy, M.S. Briggs, C.J. McKnight, L.M. Gierasch, *Biochemistry* **1989**, *26*, 2789.

[23] A.B. Chetverin, E.V. Brazhnikov, *J. Biol. Chem.* **1985**, *260*, 7817.

[24] D. Naumann, C. Schultz, J. Born, F. Rogge, H. Labischinski, *Microchim. Acta* **1988**, *1*, 379.

[25] B. Kleffel, R.M. Garavito, W. Baumeister, J.P. Rosenbusch, *EMBO J.* **1985**, *4*, 1589.

[26] R.A. Dluhy, N.A. Wright, P.R. Griffiths, *Appl. Spectrosc.* **1988**, *42*, 138.

[27] S. Frei, L. Tamm, *Biophys. J.* **1991**, *60*, 922.

[28] R. Buchet, S. Varga, N.W. Seidler, E. Molnar, A. Martonosi, *Biochim. Biophys. Acta* **1991**, *1068*, 201.

[29] A. Dong, P. Huang, W.S. Caughey, *Biochemistry* **1990**, *29*, 3303.

[30] H. Vogel, F. Jahnig, V. Hoffmann, J. Stümpel, *Biochim. Biophys. Acta* **1983**, *733*, 201.

[31] A.T. Tu, 'Spectroscopy of Biological Systems', Eds. R.J.H. Clark and R.E. Hester, John Wiley & Sons Ltd., New York, 1986, p. 47.

[32] F.S. Parker, 'Applications of Infrared, Raman and Resonance Raman Spectroscopy in Biochemistry', Plenum, New York, 1983.

[33] J. Bandekar, D.J. Evans, S. Krimm, S.J. Leach, M.M. Aine, G. Minamasian, G. Nemethy, M.S. Pottle, H.A. Scheraga, E.R. Stinson, R.W. Woody, *Int. J. Peptide Prot. Res.* **1982**, *19*, 187; S. Krimm, J. Bandekar, *Adv. Protein Chem.* **1986**, *38*, 181.

[34] M. Pezolet, L. Duschesneau, P. Bougis, J. Faucon, J. Dufourcg, *Biochim. Biophys. Acta* **1982**, *704*, 515.

[35] J.W. Brauner, R. Mendelsohn, F.G. Prendergast, *Biochemistry* **1987**, *26*, 8151.

[36] W.-J. Yang, P.R. Griffiths, D.M. Byler, H. Susi, *Appl. Spectrosc.* **1985**, *39*, 282.

[37] F. Kopp, P.A. Cuendet, in 'Liquid Crystals of One- and Two-Dimensional Order', Eds. W. Helfrich and G. Heppke, Springer, Berlin, 1980, p. 361.

[38] W. Hübner, H.H. Mantsch, *Biophys. J.* **1991**, *59*, 1261.

[39] M. Dunäch, E. Pedròs, E. Seigneuret, J.-L. Rigaud, *J. Biol. Chem.* **1988**, *263*, 7555.

[40] E. Okamura, J. Umemura, T. Takenaka, *Biochim. Biophys. Acta* **1990**, *1025*, 94.

[41] For a review see: Chemical, Biochemical and Environmental Sensors, R.A. Lieberman, M.T. Wlodarczyk, *SPIE* **1989**, *1172*.

[42] U.P. Fringeli, Hs.H. Günthard, *Appl. Opt.* **1971**, *10*, 819.

[43] M. Forster, U.P. Fringeli, Hs.H. Günthard, *Helv. Chim. Acta* **1973**, 389.

[44] Hs.H. Günthard, *Ber. Bunsenges. Phys. Chem.* **1974**, *76*, 1110.

[45] U.P. Fringeli, Hs.H. Günthard, 'Membrane Spectroscopy', Ed. E. Grell, 'Molecular Biology, Biochemistry and Biophysics', Springer, Berlin, 1981, Vol. 31, p. 270.

[46] U.P. Fringeli, 'In Situ Infrared Attenuated Total Reflection Membrane Spectroscopy', in 'Internal Reflection Spectroscopy: Theory and Application', Ed. F.M. Mirabella, Marcel Dekker, New York, 1992, in press.

[47] N.J. Harrick, 'Internal Reflection Spectroscopy', Harrick Sci. Corp., Ossining, New York, 1979.

[48] F. Goos, H. Lindberg-Hänchen, *Ann. Phys.* **1949**, *5*, 251.

[49] M. Born, E. Wolf, 'Principles of Optics', Pergamon Press, Oxford, 1983.

[50] R.D.B. Fraser, T.P. MacRae, 'Conformations in Fibrous Proteins and Synthetic Polypeptides', Academic Press, New York, 1973, Chapt. 5.

[51] R. Zbinden, 'Infrared Spectroscopy of High Polymers', Academic Press, New York, 1964.

[52] J. Michl, E.W. Thulstrup, 'Spectroscopy with Polarized Light', VCH Publ. Inc., New York, 1986.

[53] E.B. Wilson, J.C. Decius, P.C. Cross, 'Molecular Vibrations. The Theory of IR and Raman Vibrational Spectra', Mc Graw-Hill, New York, 1955.

[54] O. Kratky, *Kolloid Z.* **1933**, *64*, 213.

[55] U.P. Fringeli, M. Schadt, P. Rihak, Hs.H. Günthard, *Z. Naturforsch., A* **1976**, *31*, 1098.

[56] A. Saupe, *Z. Naturforsch., A* **1964**, *19*, 161.

[57] J. Seelig, *Q. Rev. Biophys.* **1977**, *10*, 353

[58] E. Egberts, H.J.C. Berendsen, *J. Chem. Phys.* **1988**, *89*, *3718*.

[59] H.-U. Gremlich, U.P. Fringeli, R. Schwyzer, *Biochemistry* **1983**, *22*, 4257.

[60] U.P. Fringeli, P. Leutert, H. Thurnhofer, M. Fringeli, M.M. Burger, *Proc. Natl. Acad. Sci. U.S.A.* **1986**, *83*, 1315.

[61] J. Goette, 'ATR-IR-spektroskopische Untersuchung der Lokalanästhetika-Phospholipid-Modellmembran-Interaktion und dampfdruckosmometrische Bestimmung der Assoziation von Lokalanästhetika in wässriger Lösung', ETH-Dissertation, Nr. 9721, 1992, and J. Goette, X. Perlia, U.P. Fringeli, in preparation.

[62] U.P. Fringeli, 'Biologically Active Molecules', Ed. U.P. Schlunegger, Springer, Berlin, 1989, p .241.

[63] U.P. Fringeli, *Nachr. Chem. Tech. Lab.* **1985**, *33*, 708

[64] U.P. Fringeli, *J. Membrane Biol.* **1980**, *54*, 203.

[65] U.P. Fringeli, Hs.H. Gunthard, *Biochim. Biophys. Acta* **1976**, *450*, 101

[66] U.P. Fringeli, P. Ahlström, C. Vincenz, M. Fringeli, 'Fourier and Computerized IR Spectroscopy', Eds. J. Grasselli and D. Cameron, *SPIE* **1985**, *553*, 234.

[67] P. Hofer, Kinetische und strukturelle Untersuchungen an der Acetylcholinesterase (EC 3.1.1.7) PhD Thesis, ETH 7112, 1982.

[68] U.P. Fringeli, P. Hofer, *Neurochem. Int.* **1980**, *2*, 185.

[69] K.B. Blodgett, I. Langmuir, *Phys. Rev.* **1937**, *51*, 964.

[70] H. Kuhn, D. Möbius, H. Bucher, 'Techniques of Chemistry', Eds. A. Weissberger and B. Rossiter, John Wiley & Sons, New York, 1972, I, Part IIIb, p. 577.

[71] E. Haidl, Diploma Work, University of Vienna, 1988.

[72] K. Fendler, E. Grell, M. Haubs, E. Bamberg, *EMBO J.* **1985**, *4*, 3079.

[73] R. Borlinghaus, H.-J. Apell, P. Läuger, *J. Membrane Biol.* **1987**, *97*, 161.

[74] P. Hofer, U.P. Fringeli, *Biophys. Struct. Mech.* **1979**, *6*, 67.

[75] M. Schöpflin, U.P. Fringeli, X. Perlia, *J. Am. Chem. Soc.* **1987**, *189*, 2375.

[76] Y. Boulanger, S. Schreier, L.C. Leitch, I.C.P. Smith, *Can. J. Biochem.* **1980**, *58*, 986.

[77] A. Seelig, P.R. Allegrini, J. Seelig, *Biochim. Biophys. Acta* **1988**, *939*, 267.

[78] Y. Boulanger, S. Schreier, I.C.P. Smith, *Biochemistry* **1981**, *20*, 6824.

[79] M. Auger, H.C. Jarrell, I.C.P. Smith, *Biochemistry* **1988**, *27*, 4660.

[80] For a comprehensive discussion of the literature on LA/membrane interaction see [61].

[81] D.G. Cameron, H.L. Casal, H.H. Mantsch, *Biochemistry* **1980**, *19*, 3665.

[82] For charged drug molecules, the concentration at the membrane-electrolyte interface c_i may differ from the bulk concentration c_b. The intrinsic partition coefficient is, therefore, defined as $P_{int} = \lim_{c_b \to 0} \frac{c_m}{c_i}$.

[83] H.-D. Bäuerle, J. Seelig, *Biochemistry* **1991**, *30*, 7203.

[84] H.P. Limbacher, G.D. Blickenstaff, J.H. Bowen, H.H. Wang, *Biochim. Biophys. Acta* **1985**, *812*, 268.

[85] P. Schlieper, L. Michaelis, *Biophys. Struct. Mech.* **1983**, *10*, 1.

[86] D. Papahadjopoulos, K. Jacobson, G. Poste, G. Shepherd, *Biochim. Biophys. Acta* **1975**, *394*, 504.

[87] A. Cao, E. Hantz-Brachet, B Azize, E. Taillandier, G. Perret, *Chem. Phys. Lipids* **1991**, *56*, 225.

[88] A.G. Lee, *Biochim. Biophys. Acta* **1978**, *514*, 95.

[89] Y. Kaminoh, H. Kamaya, I . Ueda, *Biochim. Biophys. Acta* **1989**, *987*, *63*.

[90] S. Ohki, *Biochim. Biophys. Acta* **1984**, *777*, 56.

[91] S. McLaughlin, H. Harary, *Biochemistry* **1976**, *15*, 1941.

[92] S. McLaughlin, 'Molecular Mechanisms of Anesthesia', Ed. B.R. Fink, 'Progress in Anesthesiology', Raven Press, New York, 1975, Vol. 1, p. 193.

[93] E.K. Rooney, A.G. Lee, *Biochim. Biophys. Acta* **1983**, *732*, 428.

[94] M.R. Eftink, R.K. Puri, M.D. Ghahramani, *Biochim. Biophys. Acta* **1985**, *813*, 137.

[95] B.W. Ninham, Y.A. Parsegian, *J. Theor. Biol.* **1971**, *31*, 405 .

[96] G. Cevc, D. Marsh, 'Phospholipid Bilayers', John Wiley & Sons, New York, 1987, p. 126. This book gives a comprehensive review of physico-chemical methods.

[97] B.O. Seraphin, Proceedings on the 1st Conf. on Modulation Spectroscopy, North Holland Publ., Amsterdam, 1973.

[98] L.A. Nafie, D.W. Vidrine, 'Double modulation Fourier transform spectroscopy', in 'Fourier Transform IR spectroscopy', Academic Press, New York, 1982, Vol. 3, p. 83.

[99] A *Bruker IFS 48* FTIR Spectrometer has been modified for low frequency modulation spectroscopy. The project was performed in collaboration with *Bruker Analytische Messtechnik*, Karlsruhe (J. Gast, A. Simon, J. Gronholz), *Spectrospin AG*, Fällanden (N. Spirig, H.W. Tschopp). It was financially supported by the *Kommission zur Förderung der wissenschaftlichen Forschung (KWF)*, Bern (Projects No. 1895.1, 2245.1).

[100] H. Susi, S.N. Timasheff, L. Stevens, *J. Biol. Chem.* **1967**, *242*, 5460.

[101] T.-J. Yu, J.L. Lippert, W.L. Peticolas, *Biopolymers* **1973**, *12*, 2161.

[102] N. Greenfield, G.D. Fasman, *Biochemistry* **1969**, *8*, 4108.

[103] U. Shmueli, W. Traub, *J. Mol. Miol.* **1965**, *12*, 205.

[104] S.D. Swanson, R.G. Bryant, *Biopolymers* **1991**, *31*, 967.

[105] M. Müller, Möglichkeiten und Grenzen der Infrarot-Spektroskopie bei der Sekundärstrukturaufklärung von Proteinen und Peptiden, ETH-Dissertation 1992, and U.P. Fringeli, M. Müller, in preparation.